

Discovery and Optimization of C-2 Methyl Imidazopyrrolopyridines as Potent and Orally Bioavailable JAK1 Inhibitors with Selectivity over JAK2

Mark Zak,^{*,†} Rohan Mendonca,[†] Mercedesz Balazs,[×] Kathy Barrett,[‡] Philippe Bergeron,[†] Wade S. Blair,[‡] Christine Chang,[‡] Gauri Deshmukh,[§] Jason DeVoss,[×] Peter S. Dragovich,[†] Charles Eigenbrot,[∞] Nico Ghilardi,^{||} Paul Gibbons,[†] Stefan Gradl,[†] Chris Hamman,[†] Emily J. Hanan,[†] Eric Harstad,[⊥] Peter R. Hewitt,[○] Christopher A. Hurley,[○] Tian Jin,[●] Adam Johnson,[‡] Tony Johnson,[○] Jane R. Kenny,[§] Michael F. T. Koehler,[†] Pawan Bir Kohli,[‡] Janusz J. Kulagowski,[○] Sharada Labadie,[†] Jiangpeng Liao,[●] Marya Liimatta,[‡] Zhonghua Lin,[×] Patrick J. Lupardus,[∞] Robert J. Maxey,[○] Jeremy M. Murray,[∞] Rebecca Pulk,[†] Madeleine Rodriguez,[×] Scott Savage,[#] Steven Shia,[∞] Micah Steffek,[∞] Savita Ubhayakar,[§] Mark Ultsch,[∞] Anne van Abbema,[‡] Stuart I. Ward,[○] Ling Xiao,[●] and Yisong Xiao[●]

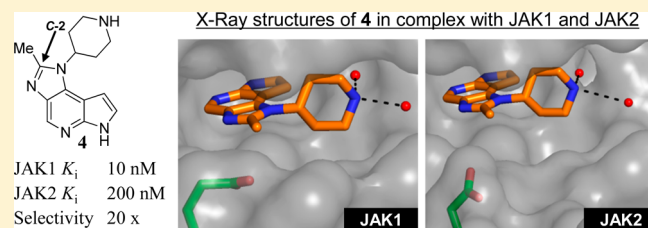
Departments of [†]Discovery Chemistry, [‡]Biochemical and Cellular Pharmacology, [§]Drug Metabolism and Pharmacokinetics, ^{||}Immunology, [⊥]Safety Assessment, [#]Small Molecule Process Chemistry, [∞]Structural Biology, and [×]Translational Immunology, Genentech, Inc., 1 DNA Way, South San Francisco, California 94080, United States

[○]Argenta, 8/9 Spire Green Centre, Flex Meadow, Harlow, Essex, CM19 5TR, United Kingdom

[●]WuXi AppTec Co., Ltd., 288 Fute Zhong Road, Waigaoqiao Free Trade Zone, Shanghai 200131, P. R. China

S Supporting Information

ABSTRACT: Herein we report the discovery of the C-2 methyl substituted imidazopyrrolopyridine series and its optimization to provide potent and orally bioavailable JAK1 inhibitors with selectivity over JAK2. The C-2 methyl substituted inhibitor **4** exhibited not only improved JAK1 potency relative to unsubstituted compound **3** but also notable JAK1 vs JAK2 selectivity (20-fold and >33-fold in biochemical and cell-based assays, respectively). Features of the X-ray structures of **4** in complex with both JAK1 and JAK2 are delineated. Efforts to improve the in vitro and in vivo ADME properties of **4** while maintaining JAK1 selectivity are described, culminating in the discovery of a highly optimized and balanced inhibitor (**20**). Details of the biological characterization of **20** are disclosed including JAK1 vs JAK2 selectivity levels, preclinical in vivo PK profiles, performance in an in vivo JAK1-mediated PK/PD model, and attributes of an X-ray structure in complex with JAK1.



INTRODUCTION

The Janus protein tyrosine kinases (JAK1,¹ JAK2,² JAK3,³ and TYK2⁴) are key intracellular mediators of helical cytokine⁵ signaling pathways. The cytokine ligands signal to cells by interacting with the extracellular portions of homo- or heterodimeric cell surface transmembrane receptors,⁶ which are further engaged with JAKs in their cytoplasmic domains. Upon ligand binding, these receptors induce activation of the associated JAKs, a mandatory initial step for all downstream signaling events, since the receptors themselves have no intrinsic kinase activity. JAK activation results in a cascade of phosphorylation and recognition events that culminate in the phosphorylation, dimerization, and nuclear translocation of one or several signal transducer and activator of transcription (STAT)⁷ proteins. Once inside the nucleus, the STATs modulate gene transcription and expression.⁸

The JAKs are activated in specific patterns by different cytokines that play essential roles in immune function,⁹ inflammation,¹⁰ and hematopoiesis.¹¹ For example, members of the γ common (γ_c) subfamily, namely, interleukins IL-2, IL-4, IL-7, IL-9, IL-15, and IL-21, activate JAK1 and JAK3 but never JAK2 or TYK2.¹² The importance of the γ_c cytokines to the immune system is highlighted by the observation of SCID (severe combined immunodeficiency) when loss of function mutations occur in the γ_c chain or JAK3.¹³ Another large subfamily of cytokines shares the glycoprotein 130 (gp130) signal transducing subunit and includes IL-6, IL-11, IL-27, and several other cytokines. Signaling by these cytokines always involves JAK1 activation, and JAK2 and TYK2 are also consistently engaged.¹⁴ IL-6 is heavily implicated in immune

Received: May 5, 2012

response, and excessive stimulation of this pathway is linked to various autoimmune and chronic inflammatory conditions.¹⁵ Finally, the receptor for erythropoietin (EPO) represents a subfamily of homodimeric receptors that also includes the receptors for prolactin, thrombopoietin, and growth hormone. The EPO pathway activates JAK2 exclusively¹⁶ and is essential to red blood cell formation or erythropoiesis.¹⁷

Each JAK isoform is employed by multiple cytokine pathways, and by extension, the biological activities of many cytokines may be abrogated by inhibition of a single JAK isoform. Since several of these cytokine activities regulate immune function, targeted inhibition of JAKs offers an attractive opportunity for therapeutic intervention against rheumatoid arthritis (RA) and other immunologic disorders. A number of small molecule JAK inhibitors have been evaluated in clinical trials for the treatment of RA, including tofacitinib/CP-690,550 (**1**)^{18–21} and ruxolitinib/INCB018424 (**2**).^{22–24} The preclinical characteristics of both molecules, including the JAK isoform potency and selectivity, have been extensively profiled by other groups.^{25,26} Consistent with these previously reported results, our biochemical assays show that **1** inhibits JAK1, JAK2, and JAK3 to an approximately equal extent and is less potent against TYK2, while **2** is a JAK1, JAK2, and TYK2 inhibitor with reduced potency against JAK3 (Figure 1). The

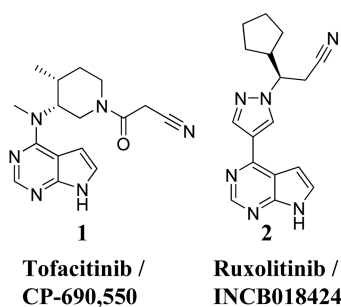
show significant activity in both cell-based assays. Each molecule's IL6-pSTAT3 EC₅₀ is less than 55 nM and is within ± 2 -fold of its corresponding EPO-pSTAT5 value, indicating potent inhibition of both JAK1 and JAK2 function in TF-1 cells.

Both **1** and **2** have demonstrated clinical efficacy in patients suffering from RA.^{20,21,23a,24} Although suppression of JAK3 and TYK2 activity may contribute to these favorable clinical outcomes, several lines of evidence point to JAK1 inhibition playing a critical and potentially dominant role. The first evidence comes from the divergent in vitro potency profiles of these compounds against the individual Janus kinase family members. Compounds **1** and **2** have considerably reduced potency against either TYK2 or JAK3, respectively, demonstrating that significant suppression of those kinase activities is likely not a prerequisite to observing clinical modulation of immune function. The second piece of evidence comes from the biology surrounding the proinflammatory cytokine IL-6. Although IL-6 activates three Janus family members (JAK1, JAK2, and TYK2), knockout studies in mice show that JAK1 is especially important to signal transduction. Indeed, after IL-6 stimulation, cells from JAK1 deficient mice show profound reductions in downstream signaling compared to wild type, whereas cells deficient in TYK2 or JAK2 maintain robust IL-6 responsiveness.^{28–30} The clinical success of the biological agent tocilizumab³¹ against RA is therefore consistent with the hypothesis that selective JAK1 inhibition will lead to therapeutic immune modulation. Tocilizumab is a neutralizing antibody directed against the IL-6 receptor α chain and is believed to exert its therapeutic effects by inhibiting the activity of the JAK1 dependent cytokine IL-6. The final evidence supporting JAK1 as an appropriate target for immune modulation comes from recent work suggesting that JAK1 rather than JAK3 kinase function is dominant in driving the activity of the immunorelevant γ_c cytokines.³²

On the basis of the above lines of evidence, we believed that a selective JAK1 inhibitor would provide efficacy against RA. We further believed that an ideal RA therapy would minimize inhibition of JAK2. JAK2 plays an integral role in the EPO signaling pathway necessary for red blood cell formation, and its inactivation leads to anemia in animal models.^{30,33} Additionally, hemoglobin reduction and anemia have been noted in human patients enrolled in clinical trials of compounds **1** and **2**, both potent inhibitors of JAK2 activity.^{20,34} The authors describing the results of one such trial note that hemoglobin reductions at higher doses of tofacitinib (>5 mg b.i.d.) may be the result of effects on hematopoiesis due to JAK2 inhibition.^{20a} On the basis of the published clinical results, we believed that even subtle selectivity for JAK1 over JAK2, on the order of 5- to 10-fold, could widen the therapeutic index for JAK1 mediated anti-RA effects relative to JAK2 dependent anemia. We therefore embarked on a program to identify potent and orally bioavailable small molecule inhibitors of JAK1, with selectivity over JAK2,³⁵ as potential therapies for RA and other immunologic disorders.

RESULTS AND DISCUSSION

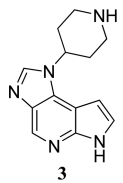
The discovery of the imidazopyrrolopyridine **3** (Figure 2) represented an important initial step in our JAK1 program.^{36,37} As previously reported,³⁶ **3** was found to be a moderately potent biochemical inhibitor of JAK1 ($K_i = 46$ nM) with reduced potency for JAK2 ($K_i = 250$ nM), resulting in a



JAK1 $K_i^{a,b}$ (nM)	0.7	0.2
JAK2 $K_i^{a,b}$ (nM)	0.7	0.1
JAK3 $K_i^{a,b}$ (nM)	0.4	3.2
TYK2 $K_i^{a,b}$ (nM)	7.8	0.5
IL6-pSTAT3 ^{b,c} (EC ₅₀ , nM)	53	24
EPO-pSTAT5 ^{b,d} (EC ₅₀ , nM)	93	12

Figure 1. Inhibition of biochemical and cell-based JAK activity by **1** and **2**. Superscript letters indicate the following: (a) biochemical assays; (b) arithmetic mean of at least three separate runs ($n \geq 3$), where on average, the coefficients of variation were less than 0.3 times the mean for biochemical assays and less than 0.5 times the mean for cell-based assays; (c) cell-based measure of JAK1 inhibition; (d) cell-based measure of JAK2 inhibition.

JAK1 and JAK2 biochemical results are supported by our cell-based measures of both JAK1 and JAK2 potency. Phosphorylation of STAT3 in TF-1 cells following IL-6 stimulation is driven predominantly by JAK1 kinase activity and forms the basis of our cellular assessment of JAK1 inhibition (IL6-pSTAT3 assay).²⁷ The corresponding assessment of cellular JAK2 inhibition is also carried out in TF-1 cells but relies on measurement of phospho-STAT5 levels following EPO stimulation (EPO-pSTAT5 assay).²⁷ Compounds **1** and **2**



JAK1 $K_i^{a,b}$ (nM)	46
JAK2 $K_i^{a,b}$ (nM)	250
JAK1 Selectivity Index (biochemical) ^a	5.4
IL6-pSTAT3 ^{d,e} (EC_{50} , nM)	1400
EPO-pSTAT5 ^{e,f} (EC_{50} , nM)	>8800 ^e
JAK1 Selectivity Index (cell-based) ^g	>6.3

Figure 2. Structure of compound **3** and inhibition of biochemical and cell-based JAK1/JAK2 activity. Superscript letters indicate the following: (a) biochemical assays; (b) arithmetic mean of eight separate runs ($n = 8$), where on average, the coefficients of variation were less than 0.3 times the mean for biochemical assays; (c) $K_i(\text{JAK2})/K_i(\text{JAK1})$; (d) cell-based measure of JAK1 inhibition; (e) arithmetic mean of three separate runs ($n = 3$), where on average, the coefficients of variation were less than 0.5 times the mean for cell-based assays; (f) cell-based measure of JAK2 inhibition; (g) see ref 38; (h) $EC_{50}(\text{EPO-pSTAT5})/EC_{50}(\text{IL6-pSTAT3})$.

biochemical JAK1 selectivity index ($K_i(\text{JAK2})/K_i(\text{JAK1})$) of 5.4-fold. Compound **3** also showed modest potency in the cell-based measurement of JAK1 inhibition (IL6-pSTAT3 $EC_{50} = 1400$ nM). Similar to the biochemical assay results, **3** was less potent in the cell-based measure of JAK2 inhibition (EPO-pSTAT5 $EC_{50} > 8800$ nM). Since its low potency precluded definitive assessment of EC_{50} in the JAK2-driven EPO-pSTAT5 assay,³⁸ it was not possible to report the unequivocal cell-based JAK1 selectivity index of **3** ($EC_{50}(\text{EPO-pSTAT5})/EC_{50}(\text{IL6-pSTAT3})$), beyond stating that it was greater than 6.3-fold. Intrigued by the emerging JAK1 selectivity displayed by compound **3**, we wished to synthesize related analogues with similar selectivity but improved potency.

During the optimization campaign of inhibitor **3**, a very promising C-2 methyl substituted analogue **4** was identified. As shown in Table 1, compound **4** exhibited notably increased biochemical inhibition of JAK1 ($K_i = 10$ nM), with only a minimal gain against JAK2 ($K_i = 200$ nM) relative to the demethyl analogue **3**. The larger increase in JAK1 relative to JAK2 inhibition of compound **4** resulted in another positive outcome, namely, increased JAK1 selectivity (biochemical JAK1 selectivity indexes: **3**, 5.4-fold; **4**, 20-fold). Also of note, the C-2 methyl group's amplification of biochemical JAK1 inhibition was mirrored in the cell-based measure of JAK1 potency (IL6-pSTAT3 EC_{50} : compound **3**, 1400 nM; compound **4**, 250 nM). The weak potency of both compounds **3** and **4** in the cellular measure of JAK2 inhibition (EPO-pSTAT5 EC_{50} : compound **3**, >8800 nM; compound **4**, >8200 nM)³⁸ precluded a definitive conclusion on the impact of the C-2 methyl group on the cell-based JAK1 selectivity index. However, it is likely that the cell-based JAK1 selectivity index of compound **4** (>33-fold) was greater than that of **3** (>6.3-fold).

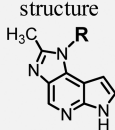
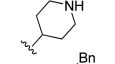
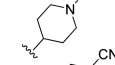
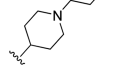
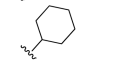
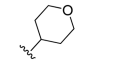
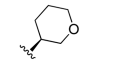
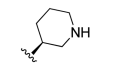
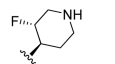
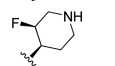
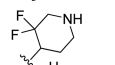
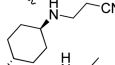
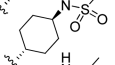
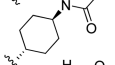
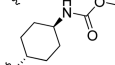
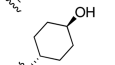
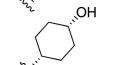
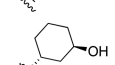
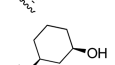
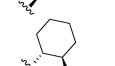
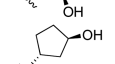
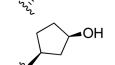
Despite the promising selectivity profile and increased JAK1 inhibition relative to its C-2 unsubstituted counterpart, compound **4** was still not an ideal development candidate. A further increase in cell-based potency was desired, and furthermore, **4** displayed poor apparent permeability as measured by flux through MDCK cells in transwell culture ($A/B P_{app} = 0.4 \times 10^{-6}$ cm/s). The low permeability elicited concern that **4** would be poorly absorbed through the intestine after oral dosing, thus potentially limiting its oral bioavailability (vide infra). The topological polar surface area (TPSA)³⁹ of compound **4** was relatively low (58 Å²), pointing toward a very low measured $\log D_{7.2}$ (0.1) as the probable explanation for the

recalcitrant permeability. As such, a series of analogues (**5–9**) with increased $\log D_{7.2}$ ⁴⁰ was synthesized. Additionally, as a means to further enhance permeability, these initial derivatives were all designed to contain only a single hydrogen-bond donor (HBD), one less than in compound **4**.

As hoped, increasing the $\log D_{7.2}$ of the single HBD-containing analogues resulted in MDCK permeability improvements to the moderate (**6** and **9**) or high (**5**, **7**, and **8**) range (Table 1). A trend in the opposite direction was identified for human hepatocyte stability, with the most lipophilic compounds **5** and **7** exhibiting the worst metabolic stability. Fortunately, compound **6** balanced moderate permeability with excellent stability in human hepatocytes, demonstrating that an optimal range of physicochemical properties existed in this series. The initial series of analogues (**5–9**) also highlighted the fact that JAK1 biochemical and cell-based potency could be maintained or improved relative to **4** with a wide array of 4-piperidine replacements. The JAK1 selectivity indexes, however, were all significantly eroded by replacing the 4-piperidine group resident in **4** with any of the HBD-lacking R-groups listed in Table 1. In fact, the three compounds with improved cellular potency (**5**, **6**, and **7**) all exhibited cell-based JAK1 selectivity indexes of less than 5-fold. These findings indicated that combining the C-2 methyl group with a HBD-containing R-group could be important to JAK1 selectivity. As such, focus was shifted to preparing additional analogues of **4** with R-groups containing HBD moieties.

In an attempt to balance optimal properties, lipophilicity restraints were put in place in the subsequent design of compounds **10–24**, with $\log D_{7.2}$ ⁴⁰ values higher than that of compound **4** (permeability considerations) but lower than those of compounds **5** and **7** (metabolic stability concerns) targeted for the majority of analogues. The 3-substituted piperidine **10** was found to be more lipophilic than the corresponding 4-substituted analogue (**4**), presumably because of closer proximity of the basic center to the electron-withdrawing tricyclic system. However, **10** displayed a large loss in biochemical JAK1 potency with only minimal gain in MDCK permeability relative to **4**. Increasing $\log D_{7.2}$ and modulating the basicity of the 4-piperidine group with fluorine atoms proved to be a more fruitful line of investigation. The *trans*-monofluoro analogue **11** displayed superior biochemical and cell-based JAK1 potency relative to its *cis* counterpart **12** and the starting point compound **4**. Additionally, compound **11** had much improved MDCK permeability relative to **4**, and although JAK1 vs JAK2 selectivity was somewhat diminished, reasonable JAK1 biochemical and cell-based indexes were maintained (5.3-fold and 15-fold, respectively). The difluorinated piperidine **13** also had improved MDCK permeability relative to **4**. Among the *trans*-1,4-diaminocyclohexanes examined (**14–17**), only the most lipophilic analogue (compound **17**) was found to exhibit high levels of MDCK permeability. Unfortunately the promising MDCK permeability of compound **17** came at the expense of reduced stability in human hepatocytes relative to compound **4**. Although a related example (compound **14**) displayed suboptimal permeability, it was modestly enhanced relative to **4**. Biochemical and cell-based JAK1 potency were also improved, while excellent human hepatocyte stability was maintained. These findings, coupled with respectable JAK1 selectivity indexes (biochemical, 6.2-fold; cell based, 15-fold), allowed **14** to remain of interest for further progression. Compounds **15** and **16**, bearing *N*-sulfonylmethyl and *N*-acetyl moieties, respectively, both lost significant potency in the cell-

Table 1. In Vitro Biological and Physical Properties of Imidazopyrrolopyridine Analogues

compd ^a	structure 	JAK1 $K_i^{b,c}$ (nM)	JAK2 $K_i^{b,c}$ (nM)	JAK1 selectivity index (biochem) ^d	IL6-pSTAT3 JAK1-cell ^{c,e} EC ₅₀ (nM)	EPO-pSTAT5 JAK2-cell ^{c,f} EC ₅₀ (nM)	JAK1 selectivity index (cell) ^g	log $D_{7.2}^h$ (measured)	TPSA (Å ²) ⁱ	MDCK P _{app} A/B ^j (x10 ⁻⁶ cm/s)	human hepatocyte ^k ($t_{1/2}$, h)
4		10 ^l	200 ^l	20	250	>8200 ^m	>33	0.1	58	0.4	>8.0
5		1.3	2.9	2.2	35	170	4.9	3.3	49	17	0.6
6		0.9	2.1	2.3	26	97	3.7	1.3	73	5.1	>8.0
7		1.3	5.0	3.8	100	490	4.9	3.3	46	20	2.3
8		18	66	3.7	990	>6800 ^m	>6.9	1.6	55	14	3.3
9 ⁿ		2.8	12	4.3	350	2300	6.6	1.8	55	7.8	6.3
10		150	580	3.9	ND ^o	ND ^o	ND ^o	0.6	58	0.8	>8.0
11 ^p		1.2	6.4	5.3	57	840	15	1.2	58	5.0	1.8
12 ^p		9.3 ^q	74 ^q	8.0	490	5400 ^r	11	0.7	58	ND ^o	ND ^o
13 ^s		2.0	11	5.5	350	2200	6.3	1.8	58	3.0	3.1
14		1.5	9.3	6.2	110	1600	15	0.9	82	0.7	>8.0
15		4.5	11	2.4	890	2800	3.1	1.2	92	0.3	>8.0
16		6.1 ^q	17 ^q	2.8	3600	>10000 ^{m,r}	>2.8	1.1	75	0.5	ND ^o
17		2.6	12	4.6	280	1700	6.1	2.0	84	12	3.9
18		5.8	24	4.1	270	2200	8.1	1.4	66	2.1	>8.0
19		6.7	18	2.7	250	2300	9.2	1.4	66	4.8	>8.0
20		1.8	12	6.7	87	1600	18	1.8	66	7.0	7.7
21 ^p		7.3	21	2.9	310	1500	4.8	1.6	66	4.9	ND ^o
22 ^p		90	520	5.8	ND ^o	ND ^o	ND ^o	1.6	66	7.7	>8.0
23 ^p		4.8	26	5.4	180	1400	7.8	1.0	66	3.6	0.9
24 ^p		5.4	28	5.2	190	800	4.2	1.2	66	5.5	5.0

^aUnless otherwise indicated, all compounds are single isomers. Where the possibility of chirality exists, data from only the most potent enantiomer are shown. ^bBiochemical assays. For brevity, only JAK1 and JAK2 data are reported. JAK3 and TYK2 inhibition data may be found in the Supporting Information. ^cUnless otherwise noted, all biochemical and cell-based assay results are reported as the arithmetic mean of at least three separate runs ($n = 3$). On average, the coefficients of variation were less than 0.3 times the mean for biochemical assays and less than 0.5 times the mean for cell-based assays. ^d $K_i(\text{JAK2})/K_i(\text{JAK1})$. ^eCell-based JAK1 assay. ^fCell-based JAK2 assay. ^g $\text{EC}_{50}(\text{EPO-pSTAT5})/\text{EC}_{50}(\text{IL6-pSTAT3})$. ^hMeasured log of distribution coefficient between octanol and aqueous pH 7.2 buffer. ⁱTopological polar surface area.³⁹ ^jApparent permeability in MDCK transwell culture. A/B, apical-to-basolateral. ^kIn vitro stability in cryopreserved human hepatocytes. ^lArithmetic mean of 11 runs ($n = 11$) ^mSee ref 38. ⁿAbsolute stereochemistry assigned arbitrarily. ^oNot determined. ^pRelative stereochemistry known but absolute stereochemistry assigned arbitrarily. ^q $n = 2$. ^r $n = 1$. ^sRacemic mixture.

based assays. A series of hydroxylated cyclohexanes (**18–22**) and cyclopentanes (**23** and **24**) as replacements for the 4-piperidine group of **4** was subsequently examined. Similar to previous examples, the regio- and stereochemistries of the hydroxyl substituents were important in modulating potency and selectivity. The *trans*-3-hydroxy analogue **20** struck the best balance among the hydroxylated derivatives and exhibited excellent biochemical and cell-based potency, acceptable JAK1 selectivity indexes (biochemical, 6.7-fold; cell-based, 18-fold), and greatly improved membrane permeability (MDCK A/B, 7.0×10^{-6} cm/s) relative to the starting point **4**. **20** also exhibited a high degree of stability in human hepatocytes. By comparison, the remaining cyclohexanol isomers (**18**, **19**, **21**, and **22**) and cyclopentanol analogues (**23** and **24**) lost varying degrees of JAK1 potency and selectivity.

The biochemical and cell-based measures of JAK1 and JAK2 inhibition led to similar conclusions about JAK1 vs JAK2 selectivity of the compounds in Table 1. Although there was a trend toward subtly increased selectivity in the cellular context, less than a 2-fold difference between biochemical and cell-based measures of selectivity for any given compound was common. Even in the most extreme case (compound **19**) only a 3.4-fold difference was observed between the biochemical and cell-based JAK1 selectivity indexes. Furthermore, the compounds with the greatest levels of cell-based selectivity (**4**, **11**, **14**, and **20**) all exhibited biochemical JAK1 selectivity indexes of greater than 5-fold, which reflected statistically significant differences in those compounds' JAK1 relative to JAK2 K_i values.⁴¹ While compound **4** was undeniably the most selective JAK1 inhibitor listed in Table 1, a number of better balanced molecules with greatly increased chances of progression as orally delivered drug candidates were identified. Notably, compounds **11**, **14**, and **20** all offered improvements in both JAK1 potency and permeability relative to **4** while retaining cell-based JAK1 selectivity indexes of 15-fold or more. Both compound **4** and a number of optimized analogues were progressed to in vivo rat PK studies to evaluate the impact of MDCK apparent permeability on oral exposure.

The in vivo rat PK parameters of reference compound **1** have been previously reported.^{19,42} As summarized in Table 2, compound **1** exhibited relatively high clearance after intravenous (iv) delivery, with oral bioavailability (F) greater than 2-fold higher than the predicted theoretical maximum (F_{\max}).⁴³ The compounds in the current work all exhibited similarly high in vivo clearance in the rat, while exposure and bioavailability varied widely after oral dosing. Two compounds (**11** and **20**) exhibited a similar profile to compound **1** in that oral bioavailability was substantially better than would be expected based on iv clearance.⁴³ It is unclear how the unexpectedly high oral exposure was achieved or whether the same mechanism was responsible for each compound.

Despite possessing an incomplete understanding of why bioavailability for certain compounds was so good in the face of high clearance, several observations allowed us to optimize oral exposure. In vitro MDCK apparent permeability did indeed appear to play an important role in influencing the in vivo oral PK parameters, with the low permeability compounds (**4** and **14**) exhibiting the poorest oral bioavailability and exposure. A combination of at least moderate permeability coupled with high solubility at pH 7.4 appeared to be the best in vitro predictor of good in vivo oral exposure. Compound **17** exhibited the best MDCK permeability but worst pH 7.4 solubility relative to the other compounds tested and exhibited

Table 2. In Vivo Rat PK Parameters and Supporting in Vitro Properties of C-2 Methylimidazopyrrolopyridine Analogues

compd	aq solubility (mM) ^a		MDCK P_{app} A/B ^b ($\times 10^{-6}$ cm/s)	MDCK P_{app} (B/A ^c)/(A/B)	% PPB (rat) ^d	rat hepatocyte ^e $t_{1/2}$ (h)	in vivo PK parameters (rat): 0.4 mg/kg (iv) and 2 mg/kg (po)						
	pH 7.4	pH 2.0					CL iv ^f (mL min ⁻¹ kg ⁻¹)	AUC po ^g (μ M·h)	C_{\max} po ^g (μ M)	F^h (%)	F_{\max}^i (%)	(% F^h)/(% F_{\max}^i)	time above EC ₅₀ ^j (h)
1							62, ^k 43 ^l	2.1 ^l	0.28, ^k 1.7 ^l	27, ^k 87 ^l	11, ^k 39 ^l	2.5, ^k 2.2 ^l	
4	>1.5	>5.0	0.4	0.7	37	>8.0	43	0.12	0.06	4	39	0.1	0
11	>1.5	ND ^m	5.0	1.2	78	1.6	40	5.3	4.5	172	43	4.0	4.0
14	>1.5	>5.0	0.7	4.0	42	>8.0	80	0.18	0.15	13	0		0
17	0.04	2.3	12	1.3	52	3.5	40	1.4	0.55	54	43	1.3	0.5
20	>1.5	>5.0	7.0	0.8	49	>8.0	43	3.4	1.3	118	39	3.0	5.6

^aThermodynamic solubility of solid powder in aqueous buffer. ^bApparent permeability in MDCK transwell culture. A/B, apical-to-basolateral. ^cB/A, basolateral-to-apical. ^dRat plasma protein binding. ^eIn vitro stability in cryopreserved rat hepatocytes. ^fIntravenous dosing. Samples **4**, **11**, **14**, **17**, and **20** were formulated as solutions in PEG400/citrate buffer (pH_{5.0}). Data are the average from three separate animals. ^gOral dosing. Samples **4**, **11**, **14**, **17**, and **20** were formulated as suspensions in MCT. Data are the average from three separate animals. ^hExperimental oral bioavailability. ⁱTheoretical maximum achievable oral bioavailability.⁴³ ^jAmount of time unbound drug plasma concentrations following 2 mg/kg po dose remained in excess of in vitro IL6-pSTAT3 EC₅₀. The unbound concentration of test compound was calculated by the equation [compound]_{unbound} = [compound]_{total}(1 - (PPB/100)). ^kData obtained or calculated from ref 19. Oral doses normalized to 2 mg/kg. ^lData obtained or calculated from ref 42. Oral doses normalized to 2 mg/kg. ^mNot determined.}

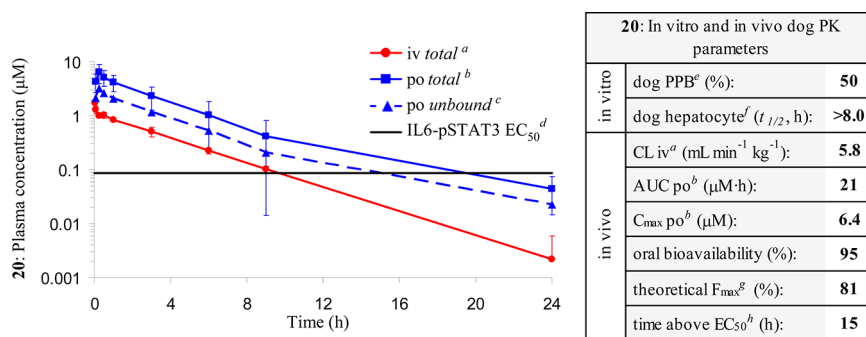


Figure 3. Exposure vs time profiles after iv and oral doses of compound **20** in the dog and relevant in vitro and in vivo parameters. Superscript letters indicate the following: (a) total plasma concentration of **20** after intravenous dosing (0.4 mg/kg), where the sample formulated as a solution in PEG400/citrate buffer (pH_{5.0}) and data are the average from three separate animals; (b) total plasma concentration of **20** after oral dosing (2 mg/kg), where the sample is formulated as a suspension in MCT and data are the average from three separate animals; (c) unbound plasma concentration of **20** after oral dosing (2 mg/kg), $[\mathbf{20}]_{\text{unbound}} = [\mathbf{20}]_{\text{total}}(1 - (\text{PPB}/100))$; (d) in vitro IL6-pSTAT3 EC₅₀ measured in TF-1 cells (87 nM); (e) dog plasma protein binding; (f) in vitro stability in cryopreserved dog hepatocytes; (g) theoretical maximum of achievable oral bioavailability (see ref 43 for calculation, and a hepatic blood flow of 30.9 mL min⁻¹ kg⁻¹ in the dog is assumed); (h) amount of time unbound drug plasma concentration following 2 mg/kg po dose remains in excess of in vitro IL6-pSTAT3 EC₅₀.

Table 3. In Vitro Measures of Either JAK1 Inhibition or Off-Target Activities of Compound 20

compd	IL6-pSTAT3 whole blood, ^a EC ₅₀ (nM)	reversible CYP inhibition, IC ₅₀ (μM)	evidence of time-dependent CYP inhibition?	hERG: % inhibition at 10 μM ^e	JAK3 K _i ^f (nM)	TYK2 K _i ^f (nM)	no. of non-JAK kinases ^h	% inhibition at 0.1 μM ^h	
20	160 ^b	>10 ^c	no ^{c,d}	8.4	22 ^g	6.2 ^g	170	→	<50
							6 ⁱ	→	50–75
							2 ^j	→	>75

^aIn vitro IL6-pSTAT3 cell-based assay conducted in TF-1 cells in the presence of human whole blood. ^bArithmetic mean of eight separate runs with eight separate blood donors. ^cCYP isoforms tested (LCMS/MS probes used): 3A4 (testosterone and midazolam), 2C9 (warfarin), 2D6 (dextromethorphan), 2C19 (mephenytoin), 1A2 (phenacetin). ^dAbsence of shift in AUC of the CYP inhibition curve of **20** with and without NADPH preincubation. ^ePatch clamp assay conducted by ChanTest. ^fBiochemical assays. ^gArithmetic mean of six separate runs. ^hOff-target kinase inhibition assessed by SelectScreen Kinase Profiling Services (Invitrogen-Life Technologies, Madison, WI, U.S.). JAK1 was included as a positive control and exhibited >95% inhibition at the concentration of **20** tested (0.1 μM). ⁱNon-JAK kinases exhibiting 50–75% inhibition at 0.1 μM **20**: CSF1R, MAP2K1, MINK1, cRAF, RSK3, RSK4. ^jNon-JAK kinases exhibiting >75% inhibition at 0.1 μM **20**: SGK3, LRRK2.

intermediate levels of oral exposure and bioavailability. By comparison, **11** and **20** balanced moderate permeability with excellent pH 7.4 solubility and achieved high levels of oral bioavailability and exposure. To help benchmark the potential biological relevance of these oral exposures, unbound plasma concentrations following oral dosing were compared to the corresponding in vitro EC₅₀ values in the IL6-pSTAT3 cell-based assay. The oral exposure profiles of compounds **4** and **14** were not sufficient to reach even transient maximum concentrations of free drug in excess of the corresponding IL6-pSTAT3 EC₅₀ values. The greatly improved permeability of **17** relative to **4** and **14** translated to significantly better oral exposure, and consequently, unbound plasma concentrations of this compound exceeded the IL6-pSTAT3 EC₅₀ for a portion of the dosing interval (0.5 h). The optimized R-groups of compounds **11** and **20** resulted in yet greater improvements to oral PK parameters, with notable increases to AUC, C_{max}, and bioavailability relative to **4**. The oral PK profiles of **11** and **20**, coupled with their potent cell-based inhibition of JAK1 activity, were sufficient to maintain unbound plasma concentrations in excess of IL6-pSTAT3 EC₅₀ for 4.0 and 5.6 h, respectively. Despite the relatively high iv clearance of compound **20** in the rat, we were encouraged by the observed level of target coverage after a single and relatively modest oral dose (2 mg/kg) and thus subjected it to further in vivo characterization.

The plasma concentration vs time curves after both oral and iv administration of compound **20** in the dog as well as relevant

in vitro and in vivo PK parameters are shown in Figure 3. As observed in other species, **20** exhibited low dog plasma protein binding (50%) as well as excellent in vitro hepatocyte stability ($t_{1/2} > 8.0$ h). Gratifyingly, compound **20** also exhibited favorable in vivo PK characteristics in the dog, with low iv clearance (5.8 mL min⁻¹ kg⁻¹) observed. The low iv clearance, coupled with good MDCK permeability, and high aqueous solubility were all consistent with the excellent oral bioavailability observed for compound **20**. Indeed, the experimental bioavailability (95%) was only marginally higher than the theoretical F_{max} of 81%.⁴³ The oral exposure achieved by compound **20** translated to free plasma concentrations in excess of the corresponding in vitro IL6-pSTAT3 EC₅₀ value for 15 h after a single oral dose of 2 mg/kg. The excellent in vivo PK profile of compound **20** in the dog provided further impetus for additional preclinical characterization.

As shown in Table 3, compound **20** was evaluated in a number of additional in vitro assays measuring either inhibition of JAK1 or off-target activities. Compound **20** exhibited low human plasma protein binding (40% bound) and did not distribute preferentially into red blood cells and thus maintained potent activity in an in vitro TF-1 cell-based measure of JAK1 inhibition conducted in the presence of human whole blood (IL6-pSTAT3 whole blood EC₅₀ = 160 nM). Compound **20** also exhibited negligible reversible or time-dependent inhibition of cytochrome P450s (CYP) and was thus considered to be at low risk for causing CYP-mediated drug–drug interactions. Risk of in vivo QT interval

prolongation was also predicted to be low because of the lack of a significant effect in an *in vitro* hERG patch clamp assay (8.4% inhibition at 10 μM **20**). The ability of **20** to inhibit the activities of the remaining two members of the JAK family was determined in biochemical assays: JAK3 $K_i = 22$ nM and TYK2 $K_i = 6.2$ nM. Finally, inhibitor **20** was found to have high selectivity for the JAK family within the broader kinome, as revealed by the results of a screen against a panel of non-JAK kinases at 0.1 μM (>50-fold over its JAK1 K_i). Of the 178 kinases tested, most (170 kinases) were inhibited to only a minimal (<50%) extent while just eight were inhibited at a more potent level (six at 50–75% inhibition, two at >75% inhibition).

To further assess the biological activity of **20**, its ability to inhibit JAK1-mediated cytokine signaling was examined *in vivo* in a PK/PD experiment in the mouse. As shown in Figure 4,

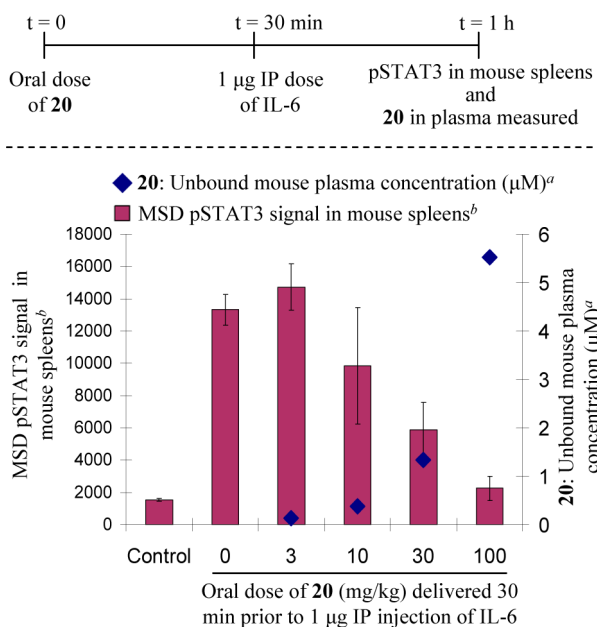


Figure 4. Design and results of an IL-6 induced pSTAT3 PK/PD study of compound **20** in the mouse (c). (a) Measured 1 h after dosing of **20**. (b) Measured 30 min after dosing of IL-6. (c) Five animals were used in each of the control and dosing arms.

mice were pretreated with ascending oral doses of compound **20** ranging from 3 to 100 mg/kg, followed by a 1 μg intraperitoneal (ip) injection of IL-6 cytokine 30 min later. An additional 30 min after IL-6 administration, concentrations of compound **20** and pSTAT3 were measured in plasma and snap-frozen spleens, respectively. As further demonstrated in Figure 4, the increasing plasma concentrations achieved with ascending oral doses of **20** in the mouse were associated with decreasing pSTAT3 levels in the spleens of IL-6 treated animals. Indeed, at a dose of 100 mg/kg **20**, pSTAT3 expression was reduced to levels comparable to those of control animals untreated with IL-6, indicating that robust *in vivo* suppression of JAK1-mediated signaling was achieved.

In an attempt to understand the intriguing effect of the C-2 methyl substituent on JAK1 potency and selectivity, X-ray crystal structures of several imidazopyrrolopyridines in the presence of JAK1 and/or JAK2 were generated. As shown in Figure 5, the first structure generated was that of compound **3** in complex with JAK2. The inhibitor occupied the ATP-binding

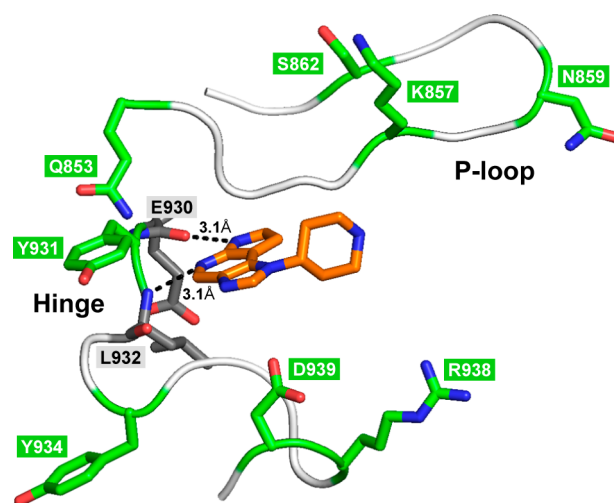


Figure 5. X-ray crystal structure of **3** in complex with JAK2 (PDB code 4F08). The ligand **3** is shown in orange. Hydrogen-bond interactions with the hinge residues L932 and E930 are shown as dashed black lines. The side chains differing between JAK1 and JAK2 are highlighted in green. The corresponding JAK1 side chains are noted in Figure 6a. The structure is of insufficient resolution (2.8 Å) to observe bound waters around the ligand.

site of JAK2, with the tricyclic core interacting with the kinase hinge region and forming hydrogen bond contacts with E930 (3.1 Å) and L932 (3.1 Å). The piperidine extended beneath the P-loop but did not form any direct polar interactions with the protein. The piperidine moiety further adopted a chair conformation, placing the tricyclic core in an equatorial position, and was rotated by approximately 90° relative to the plane of tricyclic system.

The X-ray structures of compound **4** in complex with both JAK1 and JAK2 are shown in Figure 6a and Figure 6b, respectively. The general features of both structures were similar, although subtle differences did exist. The ligand's interactions with the hinge backbone were virtually identical in both isoforms, with the pyridine N engaging either the L959 (JAK1) or L932 (JAK2) amide NH and with the pyrrole NH pairing with the E957 (JAK1) or E930 (JAK2) carbonyl oxygen. As previously observed with compound **3**, the piperidine group extending beneath the JAK P-loops adopted a chair conformation and oriented the tricyclic core in an equatorial disposition. Also similar to compound **3**, the free piperidine NH of **4** did not directly contact the JAK proteins; however, the crystal structures of **4** were of sufficient resolution to reveal its association with two crystallographic water molecules residing beneath the P-loops of JAK1 and JAK2. In the case of JAK1, these waters were tightly associated with the piperidine moiety of the ligand at distances of 2.9 and 2.8 Å, respectively, while the association was looser in JAK2, 3.2 and 3.3 Å. The weaker interactions between the ligand and the waters residing beneath the JAK2 P-loop compared to their JAK1 counterparts likely reflect a slightly less optimal fit for compound **4** in the JAK2 ATP binding pocket and may be a contributing factor to the JAK1 vs JAK2 selectivity observed for compound **4**.

A third crystallographic water molecule was observed to be associated with inhibitor **4** in the X-ray crystal structure in complex with JAK2. As shown in Figure 6b, this water molecule interacted with the available imidazole N lone pair of compound **4** at a distance of 2.8 Å. A similar interaction was

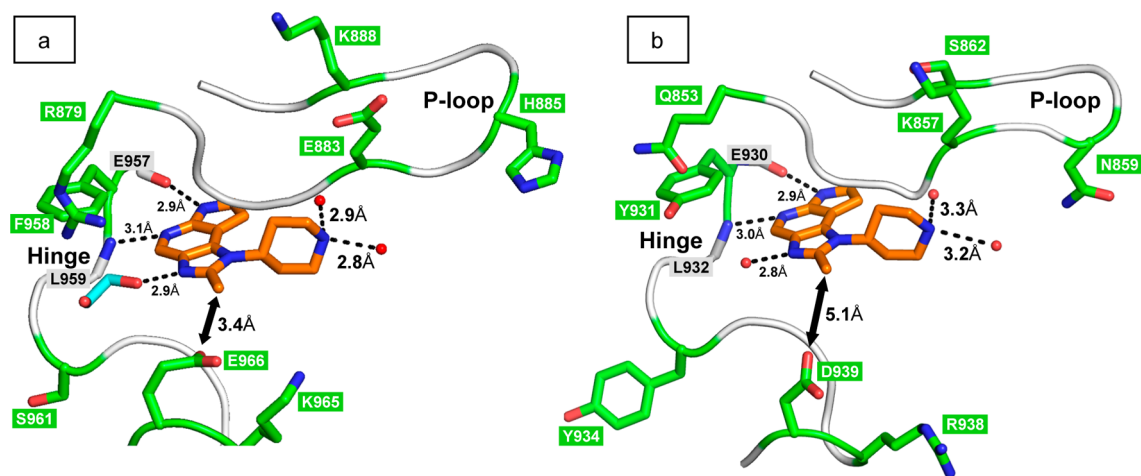


Figure 6. (a) X-ray structure of **4** in complex with JAK1 (PDB code 4EHZ). (b) X-ray structure of **4** in complex with JAK2 (PDB code 4F09). Compound **4** is depicted in orange. Hydrogen bonds to the ligand are depicted as dashed black lines. Backbone hinge atoms contacting **4** are highlighted (E957 and L959 for JAK1; E930 and L932 for JAK2). Notable crystallographic waters are denoted as red spheres (waters modeled into electron density peaks of $>1.5\sigma$). A molecule of ethylene glycol (teal) is observed in part a. The double-headed black arrows highlight the proximity of the C-2 methyl group of the ligand to a key residue difference between JAK1 (E966) and JAK2 (D939). The resolutions of the X-ray structures are 2.2 Å for JAK1 (a) and 2.4 Å for JAK2 (b).

observed in the X-ray structure of **4** in complex with JAK1 (Figure 6a), where the hydrogen bond-accepting capacity of the imidazole unit was satisfied by a molecule of ethylene glycol, a component of the crystallization solution that presumably replaced a water molecule in the crystal lattice.

The residue differences in the ATP-binding sites of JAK1 and JAK2 are highlighted in green in Figure 6a and Figure 6b. Compound **4** did not generally approach any of these closely enough to provide a clear justification for the observed isoform selectivity. One exception, however, was the E966 (JAK1) \rightarrow D939 (JAK2) residue difference. In the case of JAK2, the C-2 methyl group was too far from the D939 side chain (5.1 Å) for an interaction to take place. By contrast, in JAK1, the C-2 methyl group of **4** approached a carboxylate O-atom of the E966 side chain within 3.4 Å, a distance similar to the combined van der Waals radii of the two moieties.⁴⁴ The close approach of the C-2 methyl group to the JAK1 E966 side chain was suggestive of a potential interaction between the two groups and could be a further contributing factor to the JAK1 vs JAK2 selectivity profile of compound **4**.

In order to further understand the effect of the C-2 methyl group on JAK potency, the bound conformations of ligands **3** and **4** were examined in more detail. As shown in Figure 7, the

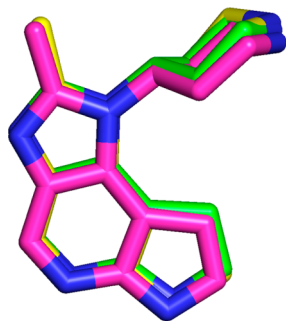


Figure 7. Bound conformations of **3** in complex with JAK2 (green) and of **4** in complex with JAK1 (pink) and JAK2 (yellow) determined by X-ray crystallography. For clarity, the structures of the proteins have been omitted.

crystallographically determined conformations of **3** in complex with JAK2 and of **4** in complex with both JAK1 and JAK2 were all found to be virtually identical. We therefore concluded that the C-2 methyl substituent was unlikely to have a large impact upon the bound conformations of ligands in either JAK1 or JAK2.

To ascertain whether the methyl group impacted *unbound* conformations, quantum mechanical (QM) calculations⁴⁵ were performed using two aqueous solvent models. As shown in Figure 8, these calculations identified two distinct local minimum energy conformations of unbound **3** and **4**. One local minimum (*out*) oriented the piperidine ring junction H atom away from the tricyclic core and was equivalent to the bound conformations observed experimentally in the X-ray structures (Figure 7). The other local minimum (*in*) rotated the piperidine moiety by 180° such that the ring junction H atom pointed toward the tricyclic core. Both QM models indicated that the experimentally observed bound conformation for compound **3** (**3_{out}**) was higher in energy than its rotational isomer **3_{in}** by 0.8 kcal/mol. Additional QM calculations using the same solvent models indicated that addition of the methyl group to the C-2 position of the tricyclic core (compound **4**) reversed the bias of the unbound ligand such that **4_{out}** was predicted to be 0.9–1.0 kcal/mol lower in energy than the rotational isomer **4_{in}**. The preference of ligand **4** for the bound conformation could contribute to its greater potency against JAK1 and JAK2 relative to compound **3**. The conformational bias of compound **4** toward the bound conformation does not, however, offer additional insight into why it is more JAK1 selective than compound **3**. We consider it likely that the observed potency and selectivity profiles are influenced by multiple factors including the ligands' interactions with crystallographic waters, the close approach of C-2 methyl substituted analogues to E966 in JAK1, and the different conformational preferences of the unbound ligands.

As shown in Figure 9, the X-ray structure of compound **20** in complex with JAK1 displayed several similar attributes to the corresponding structure of **4** (Figure 6a). The pyrrolopyridine moiety present in **20** anchored it to the L959 and E957 hinge residues of the ATP-binding site. The C-2 methyl group

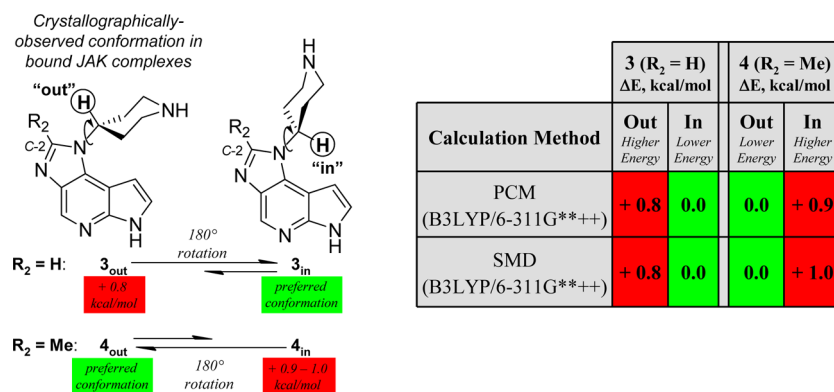


Figure 8. Relative energies of *out* vs *in* conformations of compounds **3** and **4** calculated with aqueous solvent models.⁴⁵

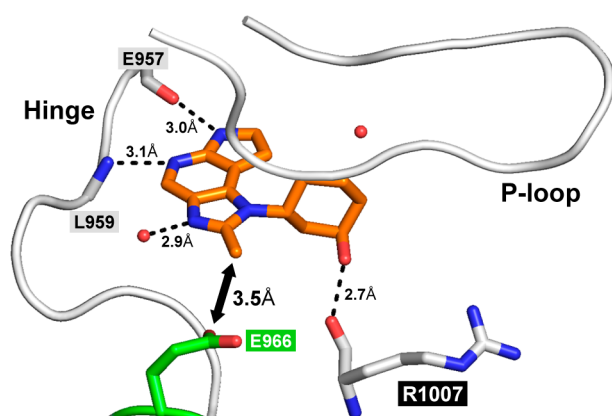


Figure 9. X-ray structure of **20** in complex with JAK1 (PDB code 4EI4). Compound **20** is depicted in orange. Hydrogen bonds to the ligand are depicted as dashed black lines. The backbone hinge atoms contacting **20** are highlighted (E957 and L959). An additional residue (R1007) forming a hydrogen bond with **20** is shown in white. Notable crystallographic waters are denoted as red spheres (waters modeled into electron density peaks of $>1.5\sigma$). The double-headed black arrow highlights the proximity of the C-2 methyl group of the ligand to a key residue difference between JAK1 (E966) and JAK2 (D939). The resolution of the X-ray structure is 2.2 Å.

resident in **20** approached the E966 side chain within 3.5 Å, again potentially contributing to the biochemical JAK1 vs JAK2 selectivity profile. The free imidazole lone pair of **20** was satisfied by an interaction with a crystallographic water observed at a distance of 2.9 Å from the ligand. Reminiscent of the piperidine moiety of compound **4**, the substituted cyclohexane ring present in **20** extended beneath the P-loop of JAK1 in a chair conformation, adopting the *out* rotational isomer and placing the tricyclic core in an equatorial disposition. As further demonstrated by Figure 9, a water molecule was observed beneath the P-loop in a location similar to one of the crystallographic waters associating with the piperidine moiety of **4**. However, unlike **4**, there was no hydrogen bond interaction between this water molecule and ligand **20**. The water was instead pushed into the back pocket by ~ 1 Å, presumably because of the hydrophobic environment created by the cyclohexane. Additionally, the axial hydroxyl group pendent to the cyclohexane ring of **20** formed a hydrogen bond with the backbone carbonyl oxygen of a residue conserved between JAK1 and JAK2 (R1007 in JAK1) at a distance of 2.7 Å. Although the corresponding X-ray structure

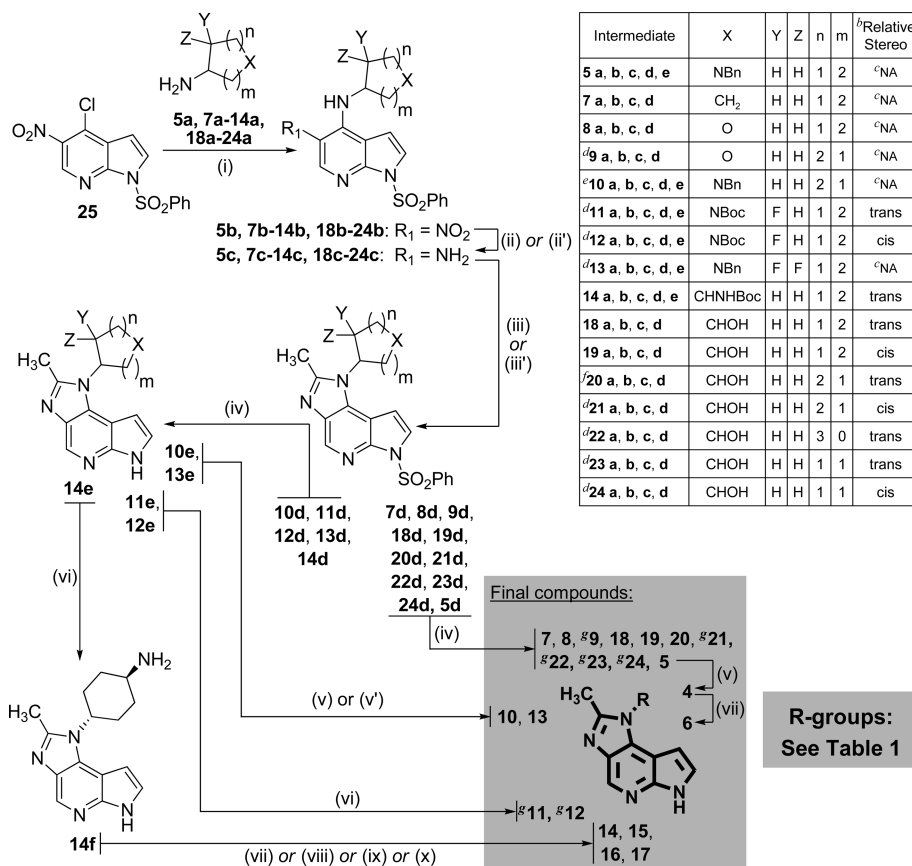
in complex with JAK2 was not generated, it is likely that a similar interaction takes place between **20** and JAK2 as well.

CHEMISTRY

As shown in Scheme 1, preparation of the C-2 methylimidazopyrrolopyridine analogues **4**–**24** commenced with S_NAr substitution of activated aryl chloride **25**³⁶ with amines **5a**, **7a**–**14a**, and **18a**–**24a** to deliver nitro anilines **5b**, **7b**–**14b**, and **18b**–**24b**. Reduction of the nitro groups under catalytic hydrogenation or reducing metal conditions led to dianilines **5c**, **7c**–**14c**, and **18c**–**24c**. Two subsequent general methods were then used to effect conversion to the corresponding C-2 methylimidazoles (intermediates **d**). The dianilines **c** could be treated with triethyl orthoacetate in the presence of acid to promote cyclization and dehydration and afford the corresponding C-2 methyl imidazoles **d**. Alternatively, it was possible to access these imidazoles by engaging the dianiline precursors **c** with an in situ generated imidate reagent produced by the action of triethylxonium tetrafluoroborate on acetamide. After imidazole formation, the **d** series of intermediates was subjected to basic hydrolysis conditions to remove the phenylsulfonamide protecting groups liberating the corresponding free indoles **10e**–**14e** and **5**, **7**–**9**, and **18**–**24**. The *N*-benzyl group protecting intermediate **10e** was removed under transfer hydrogenolysis conditions at ambient atmospheric pressure to afford *N*-unsubstituted 3-piperidine **10**. The benzyl group resident in difluoropiperidine **13e** was found to be more resilient toward deprotection, and recourse to a high pressure, continuous flow H-Cube reactor was necessary to effect its removal to afford **13**. The Boc groups protecting monofluoropiperidines **11e** and **12e** and 4-aminocyclohexane **14e** were removed with acid to provide final compounds **11** and **12** and intermediate **14f**, respectively. **14f** was converted to final products **14**, **15**, **16**, and **17** by reaction of the primary amine with acrylonitrile, methanesulfonyl chloride, acetic anhydride, and methyl chloroformate, respectively. A portion of *N*-benzyl protected piperidine **5**, prepared above, was converted to free piperidine **4** via transfer hydrogenolysis conditions under ambient atmospheric pressure. Finally, a portion of **4** was converted to **6** by alkylation of the free amine of the piperidine group with acrylonitrile.

CONCLUSION

The C-2 methyl substituted imidazopyrrolopyridine analogue **4** was found to exhibit not only increased JAK1 inhibition but also increased JAK1 vs JAK2 selectivity relative to the unsubstituted analogue **3**. Differences observed between the

Scheme 1. Preparation of C-2 Methylimidazopyrrolopyridine Analogues^a

^aReagents and conditions: (i) DIPEA, *i*-PrOH, 65–120 °C; (ii) Fe, NH₄Cl, MeOH, H₂O, reflux; (ii') H₂, Pd/C, EtOH, THF, 50 °C; (iii) triethyl orthoacetate, *p*-TsOH, toluene, reflux; (iii') acetamide, Et₃(O⁺)BF₄⁻, THF, EtOH, 25 → 70 °C; (iv) NaOH, H₂O, MeOH or EtOH, 50 °C; (v) Pd(OH)₂, ammonium formate, MeOH, 75 °C; (v') H-Cube, Pd(OH)₂ cartridge, 50 psi, 80 °C; (vi) TFA, H₂O, 25 °C; (vii) acrylonitrile, EtOH, 75 °C; (viii) MsCl, DIPEA, THF, 25 °C; (ix) Ac₂O, DIPEA, THF, 25 °C (x) methyl chloroformate, DIPEA, THF, 25 °C. ^bRelative stereochemistry between substituents on piperidine, cyclohexane, or cyclopentane rings. ^cNot applicable. ^dRacemic mixture. ^eSingle enantiomer, (*S*)-stereochemistry. ^fSingle enantiomer, (*R,R*)-stereochemistry ^gEnantiomers separated by preparative chiral SFC.

X-ray structures of compound **4** in complex with JAK1 and JAK2 suggested hypotheses for the observed selectivity profile: (1) the close approach of the C-2 methyl group of **4** to E966 in JAK1 but not D939 in JAK2; (2) the tighter association between ligand **4** and crystallographic waters under the P-loop of JAK1 compared with the corresponding waters in JAK2. Additionally, an analysis comparing the QM-calculated solution conformations of imidazopyrrolopyridines **3** and **4** to their bound X-ray structures in complex with JAK1 and/or JAK2 indicated that the C-2 methyl group's enforcement of the bound conformation likely contributed to the increased potency of **4**. Despite the increased JAK1 potency and selectivity of compound **4**, suboptimal membrane permeability limited its plasma exposure after oral administration in the rat and precluded its progression as an orally administered therapeutic. As such, an optimization campaign was undertaken in the C-2 methylimidazopyrrolopyridine series aimed at improving the permeability and oral exposure of **4** while maintaining measurable selectivity for JAK1 over JAK2. Compound **20**, the end result of this optimization effort, possessed a favorable balance of *in vitro* properties, leading to promising levels of oral exposure in the rat despite relatively high *iv* clearance. In the dog, excellent oral exposure of **20** was observed, consistent with low *iv* clearance, good MDCK permeability, and high aqueous solubility. Furthermore,

compound **20** exhibited potent inhibition in an *in vitro* cell-based measure of JAK1 activity in the presence of human whole blood (whole blood IL6-pSTAT3 EC₅₀ = 160 nM) while maintaining significant cell-based selectivity for JAK1 over JAK2 (JAK1 cell-based selectivity index of 18-fold). The combination of favorable oral PK characteristics and potent whole blood activity allowed **20** to exert a substantial effect in an *in vivo* IL6-stimulated pSTAT3 PK/PD study in the mouse. On the basis of its balanced suite of favorable physicochemical properties, its potency and selectivity for JAK1, and promising *in vivo* PK profile, compound **20** was selected for further progression in preclinical *in vitro* and *in vivo* safety studies.

EXPERIMENTAL SECTION

General. Unless otherwise indicated, all reagents and solvents were purchased from commercial sources and used without further purification. Moisture or oxygen sensitive reactions were conducted under an atmosphere of argon or nitrogen gas. Unless otherwise stated, ¹H and ¹³C NMR spectra were recorded at 298–300 K using Varian Unity Inova or Bruker Avance DRX400 instruments operating at the indicated frequencies. Chemical shifts are expressed in ppm relative to an internal standard, tetramethylsilane (0.00 ppm). The following abbreviations are used: br = broad signal, s = singlet, d = doublet, dd = doublet of doublets, t = triplet, q = quartet, m = multiplet. Unless otherwise indicated, all ¹³C peaks are singlets. Purification by silica gel chromatography was carried out using either

hand-packed glass columns or Teledyne Isco CombiFlash systems with prepacked cartridges. Some basic compounds were purified by capture on SCX (strong cation exchange) sulfonic acid cartridges, followed by elution with methanolic ammonia. Racemic mixtures of final compounds were separated into individual enantiomers by chiral SFC under the indicated conditions. Chemical and chiral (where applicable) purities were >95% for all final compounds as assessed by LCMS and chiral SFC (supercritical fluid) analysis, respectively. Further details on the analytical conditions used for individual compounds may be found in the Supporting Information. High resolution mass spectrometry (HRMS) data were collected on a Waters time of flight (LCT Premier XE) instrument using electrospray ionization.

N-(1-Benzylpiperidin-4-yl)-5-nitro-1-(phenylsulfonyl)-1H-pyrrolo[2,3-b]pyridin-4-amine (5b). A mixture of 4-chloro-5-nitro-1-(phenylsulfonyl)-1H-pyrrolo[2,3-b]pyridine (**25**)³⁶ (500 mg, 1.48 mmol), 1-benzylpiperidin-4-amine (**5a**) (337 mg, 1.78 mmol), DIPEA (380 μ L, 2.22 mmol), and *i*-PrOH (7.4 mL) was heated at 120 °C for 12 min using microwave irradiation. The cooled mixture was diluted with DCM (30 mL), loaded onto diatomaceous earth, and purified by chromatography on silica gel (gradient 0–50% EtOAc in DCM) to afford 499 mg (69%) of the title product as a yellow foam. ¹H NMR (400 MHz, CDCl₃) δ : 9.10 (m, 2H), 8.19 (d, *J* = 7.9 Hz, 2H), 7.60 (m, 2H), 7.51 (t, *J* = 7.8 Hz, 2H), 7.30 (m, 5H), 6.69 (d, *J* = 4.2 Hz, 1H), 4.00 (m, 1H), 3.57 (s, 2H), 2.85 (m, 2H), 2.31 (m, 2H), 2.11 (m, 2H), 1.79 (m, 2H). LCMS (method LCMS1, ESI) t_R = 3.35 min, *m/z* = 492.6 [M + H]⁺.

N⁴-(1-Benzylpiperidin-4-yl)-1-(phenylsulfonyl)-1H-pyrrolo[2,3-b]pyridine-4,5-diamine (5c). A mixture of **5b** (442 mg, 899 μ mol), iron powder (~325 mesh, 201 mg, 3.60 mmol), and ammonium chloride (289 mg, 5.39 mmol) was suspended in a mixture of MeOH and water (3:1, 12 mL) and was heated at reflux for 4 h. The cooled mixture was filtered through Celite, washing with MeOH (50 mL). The filtrate was concentrated under vacuum, and the resulting residue was partitioned between a saturated aqueous sodium bicarbonate solution (25 mL) and DCM (25 mL). The layers were separated. Then the aqueous phase was re-extracted with DCM (2 \times 25 mL). The combined organic extracts were washed with brine (25 mL), dried over sodium sulfate, filtered, and concentrated under vacuum to afford a dark pink residue. Purification by column chromatography on silica gel (gradient 0–10% MeOH in DCM) afforded 321 mg (77%) of the title compound as an off-white solid. LCMS (LCMS1, ESI): t_R = 2.55 min, *m/z* = 462.5 [M + H]⁺.

1-(1-Benzylpiperidin-4-yl)-2-methyl-6-(phenylsulfonyl)-1,6-dihydroimidazo[4,5-d]pyrrolo[2,3-b]pyridine (5d). A mixture of **5c** (325 mg, 0.704 mmol), triethyl orthoacetate (394 μ L, 2.16 mmol), and *p*-toluenesulfonic acid monohydrate (20.0 mg, 0.115 mmol) in toluene (10 mL) was heated to reflux for 20 h. After the mixture was cooled to room temperature, EtOAc (25 mL) was added. The organic phase was washed with a saturated aqueous solution of sodium hydrogen carbonate, water, and brine (1 \times 20 mL each), then dried over sodium sulfate, filtered, and concentrated to dryness under vacuum. Purification of the residue by column chromatography on silica gel (gradient 0–50% EtOAc in DCM) gave 301 mg (88%) of the title compound as an off-white solid. ¹H NMR (400 MHz, DMSO-*d*₆) δ : 8.79 (s, 1H), 8.23 (d, *J* = 7.8 Hz, 2H), 7.85 (d, *J* = 4.0 Hz, 1H), 7.54 (t, *J* = 7.4 Hz, 1H), 7.46 (t, *J* = 7.7 Hz, 2H), 7.39 (m, 5H), 7.31 (m, 1H), 4.36 (m, 1H), 3.62 (s, 2H), 3.13 (m, 2H), 2.66 (s, 3H), 2.58 (m, 2H), 2.21 (t, *J* = 11.7 Hz, 2H), 1.85 (m, 2H). LCMS (method LCMS1, ESI): t_R = 3.16 min, *m/z* = 486.4 [M + H]⁺.

1-(1-Benzylpiperidin-4-yl)-2-methyl-1,6-dihydroimidazo[4,5-d]pyrrolo[2,3-b]pyridine (5). A mixture of **5d** (275 mg, 566 μ mol) in MeOH (20 mL) was treated with a 1 M aqueous NaOH solution (5 mL) and stirred at room temperature for 18 h. The majority of the MeOH was removed under vacuum, and the resulting suspension was extracted with EtOAc (3 \times 20 mL). The combined organic extracts were washed with water and brine (1 \times 20 mL each), dried over sodium sulfate, filtered, and concentrated to dryness under vacuum. Purification of the residue by column chromatography on silica gel (gradient 0–10% MeOH in DCM) afforded a residue which

was triturated with diethyl ether (10 mL) to give 137 mg (70%) of the title compound as a white solid. ¹H NMR (400 MHz, DMSO-*d*₆) δ : 11.78 (s, 1H), 8.46 (s, 1H), 7.51 (t, *J* = 3.0 Hz, 1H), 7.41 (m, 4H), 7.28 (t, *J* = 7.1 Hz, 1H), 6.96 (s, 1H), 4.48 (m, 1H), 3.62 (s, 2H), 3.04 (d, *J* = 11.2 Hz, 2H), 2.62 (s, 3H), 2.57 (m, 2H), 2.23 (t, *J* = 11.7 Hz, 2H), 1.88 (d, *J* = 12.4 Hz, 2H). ¹³C NMR (125 MHz, DMSO-*d*₆) δ : 149.2, 144.2, 138.4, 134.6, 134.1, 132.0, 128.6, 128.3, 126.9, 123.6, 104.3, 99.5, 62.0, 54.9, 52.3, 29.5, 14.4. LCMS (method LCMS2, ESI): t_R = 1.83 min, *m/z* = 346.1 [M + H]⁺. HRMS [M + H]⁺ expected, 346.2032; found, 346.2061.

2-Methyl-1-(piperidin-4-yl)-1,6-dihydroimidazo[4,5-d]pyrrolo[2,3-b]pyridine (4). A mixture of **5** (1.70 g, 4.92 mmol), palladium hydroxide (20 wt % on carbon, 492 mg, 707 μ mol), and ammonium formate (4.44 g, 70.6 mmol) in MeOH (120 mL) was heated at 75 °C for 3 h. The cooled mixture was filtered through Celite and concentrated to dryness under vacuum. The residue obtained was triturated with EtOAc (10 mL) to afford the crude title compound as a beige solid (1.1 g, 87%). Then 200 mg of the crude product was purified by preparative HPLC (column, Phenomenex Gemini C18, 21.2 cm \times 250 cm, 5 μ m; detection, UV 254 nm; mobile phase A, water containing 0.1% NH₄OH; mobile phase B, CH₃CN containing 0.1% NH₄OH; flow rate of 18 mL/min; gradient 5–30% B over 15 min) and then by an Isolute SCX-2 column chromatography (gradient, MeOH to 2 M NH₃ in MeOH) to afford 78 mg of the pure title compound as a white solid. ¹H NMR (400 MHz, DMSO-*d*₆) δ : 11.73 (s, 1H), 8.45 (s, 1H), 7.43 (t, *J* = 3.0 Hz, 1H), 6.96 (s, 1H), 4.48 (s, 1H), 3.16 (d, *J* = 12.2 Hz, 2H), 2.71 (t, *J* = 12.2 Hz, 2H), 2.62 (s, 3H), 2.38 (m, 3H), 1.79 (d, *J* = 12.1 Hz, 2H). ¹³C NMR (125 MHz, DMSO-*d*₆) δ : 149.2, 144.3, 134.6, 134.1, 132.2, 123.3, 104.2, 100.1, 53.4, 45.6, 30.6, 14.5. LCMS (method LCMS2, ESI): t_R = 0.68 min, *m/z* = 256.1 [M + H]⁺. HRMS [M + H]⁺ expected, 256.1562; found, 256.1574.

3-(4-(2-Methylimidazo[4,5-d]pyrrolo[2,3-b]pyridin-1(6H)-yl)-piperidin-1-yl)propanenitrile (6). Compound **4** was treated with conditions similar to those used to convert **14f** to **14** (vide infra), to produce the title compound as a white solid. ¹H NMR (400 MHz, DMSO-*d*₆) δ : 11.73 (s, 1H), 8.45 (s, 1H), 7.42–7.35 (m, 1H), 6.94 (s, 1H), 4.48 (m, 1H), 3.12 (d, *J* = 11.3 Hz, 2H), 2.81–2.66 (m, 4H), 2.62 (s, 3H), 2.59–2.52 (m, 2H), 2.29 (t, *J* = 11.0 Hz, 2H), 1.90 (d, *J* = 8.3 Hz, 2H). LCMS (method LCMS2, ESI) t_R = 1.06 min, *m/z* = 309.1 [M + H]⁺.

N-Cyclohexyl-5-nitro-1-(phenylsulfonyl)-1H-pyrrolo[2,3-b]pyridin-4-amine (7b). A mixture of **25**³⁶ (10.0 g, 29.6 mmol), cyclohexylamine (**7a**) (3.40 mL, 30.0 mmol), and DIPEA (11.0 mL, 65.0 mmol) in *i*-PrOH (150 mL) was heated at 80 °C for 14 h. The mixture was then cooled to 25 °C and stirred for an additional 6 h. A yellow solid precipitated from solution and was collected by vacuum filtration, then washed with *i*-PrOH (1 \times 30 mL) and air-dried to afford the title compound as a yellow solid (10.45 g, 90%). ¹H NMR (400 MHz, DMSO-*d*₆) δ : 8.93 (s, 1H), 8.91 (s, 1H), 8.13 (d, *J* = 7.6 Hz, 2H), 7.82 (d, *J* = 4.1 Hz, 1H), 7.77 (t, *J* = 7.4 Hz, 1H), 7.66 (t, *J* = 7.8 Hz, 2H), 6.99 (d, *J* = 4.2 Hz, 1H), 4.12–4.01 (m, 1H), 2.02–1.93 (m, 2H), 1.76–1.54 (m, 3H), 1.55–1.38 (m, 4H), 1.33–1.20 (m, 1H). LCMS (method LCMS3, ESI): t_R = 1.33 min, *m/z* = 401.2 [M + H]⁺.

N⁴-Cyclohexyl-1-(phenylsulfonyl)-1H-pyrrolo[2,3-b]pyridine-4,5-diamine (7c). A suspension of **7b** (10.0 g, 25.0 mmol) and palladium on carbon (2.7 g, 10%, wet, Degussa, E101 NE/W) in a 3:1 mixture of THF and EtOH (200 mL) was stirred under a hydrogen atmosphere (balloon) at 50 °C for 13 h. The reaction mixture was cooled to 25 °C and then was filtered through Celite. The filtrate was concentrated under reduced pressure to afford the crude title product (9.61 g, 100%) as a rose foam. LCMS (method LCMS3, ESI): t_R = 0.83 min, *m/z* = 371.2 [M + H]⁺. This material was used in subsequent reactions without additional purification or characterization.

1-Cyclohexyl-2-methyl-6-(phenylsulfonyl)-1,6-dihydroimidazo[4,5-d]pyrrolo[2,3-b]pyridine (7d). *p*-Toluenesulfonic acid monohydrate (0.429 g, 2.26 mmol) was added to a solution of **7c** (1.04 g, 2.82 mmol) and triethyl orthoacetate (1.29 mL, 7.05 mmol) in toluene (10 mL) at 25 °C. The reaction mixture was heated

at 105 °C for 13 h, then was cooled to 25 °C and partitioned between half-saturated aqueous NaHCO₃ solution (100 mL) and a 1:1 mixture of EtOAc and heptane (2 × 125 mL). The organic layers were dried over MgSO₄, filtered, and the filtrate was concentrated under reduced pressure. Purification of the resulting solid by column chromatography on silica gel (gradient 0–8% MeOH in DCM) afforded the title product (0.572 g, 52%) as a beige solid. ¹H NMR (400 MHz, CDCl₃) δ: 8.80 (s, 1H), 8.23 (d, *J* = 7.8 Hz, 2H), 7.80 (d, *J* = 4.0 Hz, 1H), 7.55 (t, *J* = 7.4 Hz, 1H), 7.47 (t, *J* = 7.7 Hz, 2H), 7.26 (s, 1H), 6.90 (br s, 1H), 4.43–4.25 (m, 1H), 2.67 (s, 3H), 2.30–2.11 (m, 2H), 2.11–1.99 (m, 3H), 1.99–1.81 (m, 2H), 1.57–1.41 (m, 2H). LCMS (method LCMS3, ESI): *t*_R = 0.99 min, *m/z* = 395.2 [M + H]⁺.

1-Cyclohexyl-2-methyl-1,6-dihydroimidazo[4,5-*d*]pyrrolo[2,3-*b*]pyridine (7). Sodium hydroxide (10 mL of a 1.0 M aqueous solution) was added to a solution of 7d (0.574 g, 1.46 mmol) in MeOH (20 mL) at 25 °C. The reaction mixture was stirred at 50 °C for 14 h, then was cooled to 25 °C, and the majority of MeOH was removed under vacuum. The mixture was then partitioned between water (100 mL) and EtOAc (2 × 200 mL). The combined organic layers were dried over MgSO₄, filtered, and the filtrate was concentrated under reduced pressure. Purification of the residue by preparative HPLC (column, Gemini-NX, 5 cm × 10 cm, 10 μm; detection, UV 254 nm; mobile phase A, water containing 0.1% NH₄OH; mobile phase B, CH₃CN; flow rate of 18 mL/min; gradient 5–95% B over 15 min) afforded the title compound (0.181 g, 49%) as an off-white solid. ¹H NMR (400 MHz, DMSO-*d*₆) δ: 11.77 (s, 1H), 8.45 (s, 1H), 7.45 (t, *J* = 2.9 Hz, 1H), 6.71 (s, 1H), 4.53–4.35 (m, 1H), 2.62 (s, 3H), 2.34–2.18 (m, 2H), 1.92 (t, *J* = 13.8 Hz, 4H), 1.78 (d, *J* = 11.3 Hz, 1H), 1.64–1.36 (m, 3H). ¹³C NMR (125 MHz, DMSO-*d*₆) δ: 149.2, 144.2, 134.6, 134.2, 132.0, 123.3, 104.0, 99.6, 54.6, 30.1, 25.1, 24.4, 14.4. LCMS (method LCMS4, ESI): *t*_R = 3.26 min, *m/z* = 255.1 [M + H]⁺. HRMS [M + H]⁺ expected, 255.1610; found, 255.1676.

2-Methyl-1-(tetrahydro-2H-pyran-4-yl)-1,6-dihydroimidazo[4,5-*d*]pyrrolo[2,3-*b*]pyridine (8). 8 was synthesized by methods similar to those used for 7, substituting 4-aminotetrahydropyran (8a) for cyclohexylamine (7a). ¹H NMR (400 MHz, DMSO-*d*₆) δ: 11.82 (s, 1H), 8.47 (s, 1H), 7.48 (d, *J* = 3.1 Hz, 1H), 6.72 (d, *J* = 3.1 Hz, 1H), 4.75 (m, 1H), 4.11 (dd, *J* = 11.5, 4.7 Hz, 2H), 3.60 (t, *J* = 11.3 Hz, 2H), 2.65 (s, 3H), 2.60–2.49 (m, 2H), 1.87 (dd, *J* = 12.6, 4.3 Hz, 2H). LCMS (method LCMS4, ESI): *t*_R = 2.55 min, *m/z* = 257.2 [M + H]⁺.

2-Methyl-1-(tetrahydro-2H-pyran-3-yl)-1,6-dihydroimidazo[4,5-*d*]pyrrolo[2,3-*b*]pyridine (9). (±)-9 was synthesized by methods similar to those used for 7 and substituting (±)-3-aminotetrahydropyran (9a) for cyclohexylamine (7a). 9 was separated from *ent*-9 by preparative chiral SFC (column, Chiralpak AD, 2.12 cm × 25 cm, 5 μm; detection, UV 220 nm; mobile phase A, CO₂; mobile phase B, MeOH; flow rate of 50 mL/min; gradient, isocratic, A/B = 75:25). Isolation and concentration of the appropriate fractions afforded two products with the following characteristics. For 9, analytical chiral SFC (method SFC1) *t*_R = 1.12 min. ¹H NMR (400 MHz, DMSO-*d*₆) δ: 11.81 (s, 1H), 8.46 (s, 1H), 7.47 (s, 1H), 6.81 (d, *J* = 3.2 Hz, 1H), 4.61 (m, 1H), 4.01 (m, 3H), 3.75–3.56 (m, 1H), 2.65 (s, 3H), 2.56–2.46 (m, 1H, overlaps with DMSO-*d*₆), 2.09 (d, *J* = 14.7 Hz, 1H), 1.92 (m, 2H). LCMS (method LCMS4, ESI): *t*_R = 2.64 min, *m/z* = 257.1 [M + H]⁺. For *ent*-9, analytical chiral SFC (method SFC1) *t*_R = 1.28 min. ¹H NMR and LCMS data match those of 9.

(S)-2-Methyl-1-(piperidin-3-yl)-1,6-dihydroimidazo[4,5-*d*]pyrrolo[2,3-*b*]pyridine (10). 10 was synthesized by methods similar to those used for 4 and 5 and substituting (S)-1-benzylpiperidin-3-amine (10a) for 1-benzylpiperidin-4-amine (5a). ¹H NMR (400 MHz, DMSO-*d*₆) δ: 11.76 (s, 1H), 8.45 (s, 1H), 7.45 (t, *J* = 3.0 Hz, 1H), 6.86–6.76 (m, 1H), 4.49 (s, 1H), 3.10–2.92 (m, 2H), 2.74–2.65 (m, 1H), 2.63 (s, 3H), 2.45–2.30 (m, 2H), 2.01 (d, *J* = 12.1 Hz, 1H), 1.85 (d, *J* = 12.3 Hz, 1H), 1.77–1.60 (m, 1H). LCMS (method LCMS4, ESI): *t*_R = 2.05 min, *m/z* = 256.1 [M + H]⁺.

(±)-*trans*-*tert*-Butyl 3-Fluoro-4-(5-nitro-1-(phenylsulfonyl)-1H-pyrrolo[2,3-*b*]pyridin-4-ylamino)piperidine-1-carboxylate (11b). A mixture of 25³⁶ (1.77 g, 5.23 mmol), (±)-*trans*-*tert*-butyl 4-

amino-3-fluoropiperidine-1-carboxylate (11a⁴⁶) (878 mg, 4.02 mmol), and DIPEA (1.65 mL, 9.50 mmol) in *i*-PrOH (10 mL) was stirred overnight at 82 °C, then cooled to room temperature. An off-white solid precipitated from solution and was collected by filtration and washed with water to yield 1.62 g (78%) of the title compound. This material was used in the next step without further purification. ¹H NMR (400 MHz, DMSO-*d*₆) δ: 8.96–8.89 (m, 2H), 8.13 (d, *J* = 7.4, 2H), 7.86–7.83 (m, 1H), 7.76 (t, *J* = 8.0 Hz, 1H), 7.65 (t, *J* = 8.0 Hz, 2H), 7.20–7.15 (m, 1H), 4.88–4.69 (m, 1H), 4.57–4.41 (m, 1H), 4.18–4.04 (m, 1H), 3.88–3.74 (m, 1H), 3.26–3.02 (m, 2H), 2.08–1.96 (m, 1H), 1.81–1.69 (m, 1H), 1.42 (s, 9H). LCMS (method LCMS5, ESI): *t*_R = 1.22 min, *m/z* = 520.0 [M + H]⁺.

(±)-*trans*-*tert*-Butyl 4-(5-Amino-1-(phenylsulfonyl)-1H-pyrrolo[2,3-*b*]pyridin-4-ylamino)-3-fluoropiperidine-1-carboxylate (11c). 10% palladium on activated carbon (0.025 g, 0.023 mmol) was added to 11b (0.618 g, 1.19 mmol) in EtOAc (10 mL), and the mixture was stirred at 50 °C under an atmosphere of hydrogen (balloon) for 16 h. The mixture was then filtered through diatomaceous earth and the filtrate concentrated under vacuum to give 540 mg (92%) of the title compound as an off-white solid. This material was used immediately in the next step without further purification. LCMS (method LCMS5, ESI): *t*_R = 0.88 min, *m/z* = 490.0 [M + H]⁺.

(±)-*trans*-*tert*-Butyl 3-Fluoro-4-(2-methyl-6-(phenylsulfonyl)imidazo[4,5-*d*]pyrrolo[2,3-*b*]pyridin-1(6H)-yl)piperidine-1-carboxylate (11d). A mixture of 11c (0.540 g, 1.10 mmol) and triethyl orthoacetate (1.01 mL, 5.52 mmol) in acetic acid (5 mL) was heated at 120 °C for 10 min. The mixture was then cooled to room temperature and concentrated under vacuum. Purification of the residue by column chromatography on silica gel (gradient 0–100% (20% MeOH/EtOAc) in heptane) gave 476 mg (84%) of the title compound as an off-white solid. ¹H NMR (400 MHz, DMSO-*d*₆) δ: 8.66 (s, 1H), 8.16 (d, *J* = 7.3 Hz, 2H), 7.94 (d, *J* = 3.7 Hz, 1H), 7.71 (t, *J* = 7.4 Hz, 1H), 7.62 (t, *J* = 7.8 Hz, 2H), 6.48 (br, 1H), 5.17–5.08 (m, 1H), 5.02–4.93 (m, 2H), 4.48–4.35 (m, 1H), 4.19–4.07 (m, 1H), 3.22–3.05 (m, 1H), 2.63 (s, 3H), 2.31–2.19 (m, 1H), 2.19–2.08 (m, 1H), 1.49 (s, 9H). LCMS (method LCMS5, ESI): *t*_R = 1.07 min, *m/z* = 514.0 [M + H]⁺.

(±)-*trans*-*tert*-Butyl 3-Fluoro-4-(2-methylimidazo[4,5-*d*]pyrrolo[2,3-*b*]pyridin-1(6H)-yl)piperidine-1-carboxylate (11e). Sodium hydroxide (1 M aqueous solution, 5 mL) was added to a mixture of 11d (0.476 g, 0.927 mmol) in EtOH (5 mL) and tetrahydrofuran (8 mL). The reaction mixture was heated at 50 °C for 2 h. The mixture was then cooled to room temperature and concentrated under vacuum. Purification of the residue by column chromatography on silica gel (gradient 0–100% (20% MeOH/EtOAc) in heptane) gave 238 mg (69%) of the title compound as an off-white solid. ¹H NMR (400 MHz, DMSO-*d*₆) δ: 11.93 (s, 1H), 8.51 (s, 1H), 7.42 (s, 1H), 6.19 (s, 1H), 5.28–5.21 (m, 1H), 5.12–5.08 (m, 1H), 4.98–4.87 (m, 1H), 4.48–4.35 (m, 1H), 4.19–4.07 (m, 1H), 3.22–3.05 (m, 2H), 2.62 (s, 3H), 2.19–2.08 (m, 1H), 1.52 (s, 9H). LCMS (method LCMS5, ESI): *t*_R = 0.14 min, *m/z* = 374.0 [M + H]⁺.

***trans*-1-(4-Fluoropiperidin-3-yl)-2-methyl-1,6-dihydroimidazo[4,5-*d*]pyrrolo[2,3-*b*]pyridine (11).** To a mixture of 11e (238 mg, 0.637 mmol) in dioxane (5 mL) was added HCl (4 M solution in dioxane, 1 mL). The reaction mixture was stirred at room temperature for 2 h, then concentrated to dryness under vacuum to give the crude racemic title product. 11 was separated from *ent*-11 by preparative chiral SFC (column, Chiralpak IC, 21.2 mm × 250 mm, 5 μm; detection, UV 220 nm; mobile phase A, CO₂; mobile phase B, MeOH containing 0.1% DEA; flow rate of 50 mL/min; gradient, isocratic, A/B = 70:30). Isolation and concentration of the appropriate fractions afforded two products with the following characteristics. For 11, white solid (36.5 mg, 21%). Analytical chiral SFC (method SFC2): *t*_R = 0.89 min. ¹H NMR (400 MHz, DMSO-*d*₆) δ: 11.83 (s, 1H), 8.49 (s, 1H), 7.47 (s, 1H), 6.86 (s, 1H), 5.34–5.10 (m, 1H), 4.71–4.52 (m, 1H), 3.59–3.41 (m, 1H), 3.15–3.02 (m, 1H), 2.83–2.64 (m, 3H), 2.60 (s, 3H), 2.07–1.93 (m, 1H). ¹³C NMR (125 MHz, DMSO-*d*₆) δ: 150.1, 144.3, 134.8, 134.2, 131.3, 123.8, 103.9, 99.6, 88.5 (d, *J* = 176.7 Hz), 57.8 (d, *J* = 17.7 Hz), 49.6 (d, *J* = 22.3 Hz), 44.3, 30.6 (d, *J* = 5.2

H₂), 14.2. LCMS (method LCMS6, ESI): $t_R = 3.70$ min, $m/z = 274.0$ [M + H]⁺. HRMS [M + H]⁺ expected, 274.1468; found, 274.1463. For *ent*-11, white solid (31.3 mg, 18%). Analytical chiral SFC (method SFC2): $t_R = 1.24$ min. ¹H NMR and LCMS data match those for 11.

***cis*-1-(3-Fluoropiperidin-4-yl)-2-methyl-1,6-dihydroimidazo[4,5-*d*]pyrrolo[2,3-*b*]pyridine (12).** (±)-12 was synthesized by methods similar to those used for (±)-11 and substituting (±)-*cis*-*tert*-butyl 4-amino-3-fluoropiperidine-1-carboxylate (12a⁴⁶) for (±)-*trans*-*tert*-butyl 4-amino-3-fluoropiperidine-1-carboxylate (11a). 12 was separated from *ent*-12 by preparative chiral SFC (column, Chiralpak AD, 2.12 cm × 25 cm, 5 μm; detection, UV 220 nm; mobile phase A, CO₂; mobile phase B, EtOH containing 0.1% DEA; flow rate of 40 mL/min; gradient, isocratic, A/B = 65:35). Isolation and concentration of the appropriate fractions afforded two products with the following characteristics. For 12, white solid. Analytical chiral SFC (method SFC3): $t_R = 1.34$ min. ¹H NMR (400 MHz, DMSO-*d*₆) δ: 11.68 (s, 1H), 8.44 (s, 1H), 7.38 (s, 1H), 6.86 (s, 1H), 4.90 (s, 1H), 4.78 (s, 1H), 3.25–2.94 (m, 4H), 2.86–2.73 (m, 2H), 2.65 (s, 3H), 1.81 (br, 1H). LCMS (method LCMS4, ESI): $t_R = 0.75$ min, $m/z = 274.1$ [M + H]⁺. For *ent*-12, white solid. Analytical chiral SFC (method SFC3): $t_R = 1.91$ min. ¹H NMR and LCMS data match those of 12.

(±)-1-(3,3-Difluoropiperidin-4-yl)-2-methyl-1,6-dihydroimidazo[4,5-*d*]pyrrolo[2,3-*b*]pyridine (13). (±)-1-(1-benzyl-3,3-difluoropiperidin-4-yl)-2-methyl-1,6-dihydroimidazo[4,5-*d*]pyrrolo[2,3-*b*]pyridine (13e) was synthesized by methods similar to those used for 5 and substituting (±)-1-benzyl-3,3-difluoropiperidin-4-amine (13a⁴⁷) for 1-benzylpiperidin-4-amine (5a). A solution of 13e (69.0 mg, 0.181 mmol) in THF (6 mL) was hydrogenated on a ThalesNano H-Cube continuous-flow hydrogenation reactor (1 mL/min, 50 psi, 80 °C, one pass) using a 20% Pd(OH)₂/C CatCart. The effluent was collected and concentrated to dryness under vacuum. The residue was purified by preparative HPLC (column, Gemini-NX, 3 cm × 10 cm, 10 μm; detection, UV 254 nm; mobile phase A, water containing 0.1% NH₄OH; mobile phase B, CH₃CN containing 0.1% NH₄OH; flow rate of 20 mL/min; gradient 5–95% B over 15 min) to afford 25.0 mg (47%) of the title compound as a white solid. ¹H NMR (400 MHz, DMSO-*d*₆, 360 K) δ: 11.16 (br, 1H), 8.43 (s, 1H), 7.30 (d, *J* = 3.5 Hz, 1H), 6.80 (t, *J* = 3.3 Hz, 1H), 5.01 (br, 1H), 3.30 (t, *J* = 13.3 Hz, 1H), 3.23–3.04 (m, 2H), 2.94–2.82 (m, 2H), 2.63 (s, 3H), 2.62–2.54 (m, 1H), 2.04 (br, 1H). LCMS (method LCMS4, ESI): $t_R = 1.98$ min, $m/z = 292.0$ [M + H]⁺.

***trans*-*tert*-Butyl 4-(2-Methyl-6-(phenylsulfonyl)imidazo[4,5-*d*]pyrrolo[2,3-*b*]pyridin-1(6*H*)-yl)cyclohexylcarbamate (14d).** *trans*-*tert*-Butyl 4-(5-amino-1-(phenylsulfonyl)-1*H*-pyrrolo[2,3-*b*]pyridin-4-ylamino)cyclohexylcarbamate (14c) was synthesized by methods similar to those used for 7c, substituting *trans*-*tert*-butyl 4-aminocyclohexylcarbamate (14a) for cyclohexylamine (7a). A mixture of 14c (10.0 g, 20.6 mmol), triethyl orthoacetate (15.0 mL, 82.4 mmol), and acetic acid (120 mL) was heated to reflux for 20 min. After cooling to room temperature, the mixture was concentrated to dryness under vacuum. The residue was dissolved in EtOAc (150 mL), and the organic layer was washed with aqueous saturated sodium hydrogen carbonate solution (3 × 50 mL) and brine (50 mL). The organic layer was dried over sodium sulfate, filtered, and concentrated to dryness under vacuum. Purification of the residue by column chromatography on silica gel (gradient, DCM to neat EtOAc to 5% MeOH in EtOAc) and trituration (diethyl ether, 20 mL) provided 8.30 g (79%) of the title compound as a gray solid. ¹H NMR (400 MHz, CDCl₃) δ: 8.80 (s, 1H), 8.23 (m, 2H), 7.81 (d, *J* = 4.1 Hz, 1H), 7.51 (m, 3H), 6.86 (br s, 1H), 4.50 (m, 1H), 4.35 (m, 1H), 3.74 (m, 1H), 2.68 (s, 3H), 2.34 (m, 4H), 1.98 (m, 2H), 1.48 (s, 9H), 1.43 (m, 2H). LCMS (method LCMS7, ESI): $t_R = 3.29$ min, $m/z = 510.2$ [M + H]⁺.

***trans*-*tert*-Butyl 4-(2-Methylimidazo[4,5-*d*]pyrrolo[2,3-*b*]pyridin-1(6*H*)-yl)cyclohexylcarbamate (14e).** Aqueous sodium hydroxide solution (29.4 mL, 2.0 M) was added to a solution of 14d (6.00 g, 11.8 mmol) in MeOH (150 mL) and THF (150 mL). The reaction mixture was stirred at room temperature for 5 h, then extracted with DCM (3 × 75 mL). The combined organic extracts

were washed with brine (1 × 50 mL), then dried over sodium sulfate, filtered, and concentrated to dryness under vacuum. The resulting residue was triturated (DCM, 10 mL) and air-dried to afford 3.08 g (71%) of the title compound as a pale yellow solid. ¹H NMR (400 MHz, DMSO-*d*₆) δ: 11.80 (s, 1H), 8.45 (s, 1H), 7.49 (m, 1H), 6.95 (d, *J* = 7.3 Hz, 1H), 6.64 (d, *J* = 3.3 Hz, 1H), 4.42 (m, 1H), 3.56 (m, 1H), 2.63 (s, 3H), 2.35 (m, 2H), 1.96 (m, 4H), 1.51 (m, 2H), 1.42 (s, 9H). LCMS (method LCMS7, ESI): $t_R = 2.18$ min, $m/z = 370.0$ [M + H]⁺.

***trans*-4-(2-Methylimidazo[4,5-*d*]pyrrolo[2,3-*b*]pyridin-1(6*H*)-yl)cyclohexylamine (14f).** To a slurry of 14e (3.08 g, 8.34 mmol) and water (150 mL) was added trifluoroacetic acid (25 mL) at room temperature. The mixture was stirred for 2 h and then concentrated to dryness under vacuum. Purification of the residue by flash chromatography (SCX-2, gradient, MeOH to 2 M NH₃ in MeOH) afforded the title compound as a colorless oil (2.24 g, 100%) which was used directly in the next step without further purification. LCMS (method LCMS7, ESI): $t_R = 0.55$ and 0.67 min, $m/z = 270.1$ [M + H]⁺.

***trans*-3-(4-(2-Methylimidazo[4,5-*d*]pyrrolo[2,3-*b*]pyridin-1(6*H*)-yl)cyclohexylamino)propanenitrile (14).** A mixture of 14f (2.24 g, 8.34 mmol) and acrylonitrile (2.75 mL, 41.7 mmol) in EtOH (100 mL) was heated to 80 °C for 2 h. After cooling to room temperature, the reaction mixture was concentrated to dryness under vacuum. The residue was triturated with diethyl ether and EtOAc (10 mL each) and air-dried. Purification of the resulting solid by column chromatography on silica gel (gradient 0–20% [2 M NH₃ in MeOH] in DCM) followed by trituration with acetonitrile (3 mL) afforded 750 mg (28%) of the title compound as a white solid. ¹H NMR (400 MHz, DMSO-*d*₆) δ: 11.77 (s, 1H), 8.45 (s, 1H), 7.44 (t, *J* = 3.0 Hz, 1H), 6.70 (s, 1H), 4.45 (m, 1H), 2.87 (m, 2H), 2.77 (m, 1H), 2.62 (m, 5H), 2.33 (m, 2H), 2.09 (d, *J* = 12.5 Hz, 2H), 1.92 (m, 3H), 1.37 (m, 2H). ¹³C NMR (125 MHz, DMSO-*d*₆) δ: 149.3, 144.2, 134.6, 134.2, 123.5, 120.2, 104.0, 99.6, 54.3, 42.0, 31.8, 28.8, 18.4, 14.4. LCMS (method LCMS2, ESI): $t_R = 1.24$ min, $m/z = 323.2$ [M + H]⁺. HRMS [M + H]⁺ expected, 323.1984; found, 323.1999.

***trans*-*N*-(4-(2-Methylimidazo[4,5-*d*]pyrrolo[2,3-*b*]pyridin-1(6*H*)-yl)cyclohexyl)methanesulfonamide (15).** Methanesulfonyl chloride (24 μL, 0.31 mmol) was added to a solution of 14f (67.5 mg, 0.251 mmol) and triethylamine (105 μL, 0.75 mmol) in DCM (2 mL) at room temperature, and the reaction mixture was stirred for 16 h. The reaction mixture was loaded directly onto a silica gel column, eluting with a gradient of 0–10% MeOH in EtOAc. The appropriate fractions were collected and concentrated to dryness under vacuum. The residue was triturated with water (1 mL), then heated at 40 °C under vacuum for 16 h to afford the title compound as a white solid (44.1 mg, 51%). ¹H NMR (400 MHz, DMSO-*d*₆) δ: 11.78 (s, 1H), 8.45 (s, 1H), 7.47 (t, *J* = 3.0 Hz, 1H), 7.16 (d, *J* = 7.0 Hz, 1H), 6.72 (dd, *J* = 3.5, 1.9 Hz, 1H), 4.43 (m, 1H), 3.46 (m, 1H), 3.02 (s, 3H), 2.63 (s, 3H), 2.37 (m, 2H), 2.13 (d, *J* = 12.6 Hz, 2H), 1.92 (d, *J* = 12.3 Hz, 2H), 1.61 (t, *J* = 12.8 Hz, 2H). LCMS (method LCMS2, ESI) $t_R = 2.00$ min, $m/z = 348.1$ [M + H]⁺.

***trans*-*N*-(4-(2-Methylimidazo[4,5-*d*]pyrrolo[2,3-*b*]pyridin-1(6*H*)-yl)cyclohexyl)acetamide (16).** Acetic anhydride (21 μL, 0.22 mmol) was added to a mixture of 14f (54.3 mg, 0.202 mmol) and DIPEA (44 μL, 0.25 mmol) in DCM (2 mL). The reaction mixture was stirred for 1 h at room temperature, then concentrated to dryness under vacuum. The residue was purified by column chromatography on silica gel (gradient 0–10% [2 M NH₃ in MeOH] in DCM) to give the title compound (50.2 mg, 87%) as a white solid. ¹H NMR (400 MHz, DMSO-*d*₆) δ: 11.80 (s, 1H), 8.46 (s, 1H), 7.88 (d, *J* = 7.4 Hz, 1H), 7.49 (t, *J* = 3.0 Hz, 1H), 6.65 (dd, *J* = 3.4, 1.9 Hz, 1H), 4.48 (m, 1H), 3.83 (m, 1H), 2.64 (s, 3H), 2.36 (m, 2H), 2.98 (m, 4H), 1.84 (s, 3H), 1.52 (m, 2H). LCMS (method LCMS2, ESI) $t_R = 1.89$ min, $m/z = 312.1$ [M + H]⁺.

***trans*-Methyl 4-(2-Methylimidazo[4,5-*d*]pyrrolo[2,3-*b*]pyridin-1(6*H*)-yl)cyclohexylcarbamate (17).** 17 was synthesized by methods similar to those used for 16 and substituting methyl chloroformate for acetic anhydride. ¹H NMR (400 MHz, DMSO-*d*₆) δ: 11.80 (s, 1H), 8.45 (s, 1H), 7.49 (t, *J* = 3.0 Hz, 1H), 7.25 (s, 1H),

6.64 (s, 1H), 4.45 (s, 1H), 3.56 (m, 4H), 2.63 (s, 3H), 2.35 (m, 2H), 2.04 (m, 2H), 1.94 (m, 2H), 1.52 (m, 2H). ¹³C NMR (125 MHz, DMSO-*d*₆) δ: 155.9, 149.3, 144.2, 134.7, 134.1, 131.9, 123.6, 103.9, 99.3, 59.7, 53.6, 51.1, 48.5, 31.2, 14.0. LCMS (method LCMS2, ESI) *t*_R = 2.18 min, *m/z* = 328.3 [M + H]⁺. HRMS [M + H]⁺ expected, 328.1773; found, 328.1761.

trans-4-(2-Methylimidazo[4,5-*d*]pyrrolo[2,3-*b*]pyridin-1(6*H*)-yl)cyclohexanol (18). 18 was synthesized by methods similar to those used for 20 (vide infra) and substituting *trans*-4-aminocyclohexanol (18a) for (1*R*,3*R*)-3-aminocyclohexanol (20a). ¹H NMR (400 MHz, DMSO-*d*₆) δ: 11.75 (s, 1H), 8.44 (s, 1H), 7.44 (t, *J* = 2.9 Hz, 1H), 6.65 (s, 1H), 4.76 (d, *J* = 3.9 Hz, 1H), 4.46 (br s, 1H), 3.77 (br s, 1H), 2.62 (s, 3H), 2.38–2.26 (m, 2H), 2.03 (d, *J* = 11.1 Hz, 2H), 1.88 (d, *J* = 11.2 Hz, 2H), 1.67–1.46 (m, 2H). LCMS (method LCMS4, ESI) *t*_R = 2.42 min, *m/z* = 271.1 [M + H]⁺.

cis-4-(2-Methylimidazo[4,5-*d*]pyrrolo[2,3-*b*]pyridin-1(6*H*)-yl)cyclohexanol (19). 19 was synthesized by methods similar to those used for 20 (vide infra) and substituting *cis*-4-aminocyclohexanol (19a) for (1*R*,3*R*)-3-aminocyclohexanol (20a). ¹H NMR (400 MHz, DMSO-*d*₆) δ: 11.66 (s, 1H), 8.43 (s, 1H), 7.39 (d, *J* = 2.3 Hz, 1H), 7.36 (s, 1H), 4.87 (s, 1H), 4.41 (br, 1H), 4.03 (s, 1H), 2.76–2.61 (m, 2H), 2.61 (s, 3H), 1.88 (d, *J* = 13.2 Hz, 2H), 1.70 (t, *J* = 13.5 Hz, 2H), 1.61 (d, *J* = 11.7 Hz, 2H). LCMS (method LCMS4, ESI) *t*_R = 2.54 min, *m/z* = 271.1 [M + H]⁺.

(1*R*,3*R*)-3-(5-Amino-1-(phenylsulfonyl)-1*H*-pyrrolo[2,3-*b*]pyridin-4-ylamino)cyclohexanol (20c). (1*R*,3*R*)-3-Aminocyclohexanol (20a, 48.91 g, 76.3 mmol) was added to a stirred suspension of 25³⁶ (24.5 g, 72.6 mmol) and DIPEA (13.3 mL, 76.3 mmol) in MeOH (120 mL) at room temperature. The reaction mixture was heated to 65 °C and stirred at that temperature for 3 h. The mixture was then cooled to room temperature, and 10% palladium on carbon (7.6 g, 3.6 mmol) was added. The reaction mixture was pressurized to 100 psi with hydrogen and stirred at room temperature for 18 h. The reaction mixture was filtered, and the filtrate was concentrated to dryness under vacuum to afford the title compound as a thick yellow oil. LCMS (method LCMS8, ESI): *t*_R = 2.17 min, *m/z* = 387.1 [M + H]⁺. This material was used immediately without further purification or characterization in the next step.

(1*R*,3*R*)-3-(2-Methyl-6-(phenylsulfonyl)imidazo[4,5-*d*]pyrrolo[2,3-*b*]pyridin-1(6*H*)-yl)cyclohexanol (20d). Triethylxonium tetrafluoroborate (22.8 g, 116 mmol) was added to a slurry of acetamide (7.11 g, 120 mmol) in tetrahydrofuran (THF) (125 mL). The reaction mixture was stirred for 1 h at room temperature. Then a solution of 20c (31.0 g, 80.2 mmol) in EtOH (220 mL) was added. The reaction mixture was heated to 70 °C and stirred at that temperature for 2 h. The reaction mixture was then cooled to room temperature, and water (150 mL) was added. The mixture was extracted with 2-methyltetrahydrofuran (2 × 250 mL). Then the combined organic layers were dried over sodium sulfate, filtered, and concentrated to dryness. Ethanol (200 mL) was added, and the mixture was warmed to 50 °C. After a solution formed, the mixture was then cooled to room temperature, at which point a white solid precipitated. The solid was isolated by filtration, then dried under vacuum to afford the title compound (24.0 g, 73%) as a faintly yellow solid. ¹H NMR (400 MHz, CDCl₃) δ: 8.79 (s, 1H), 8.22 (d, *J* = 8.2 Hz, 2H), 7.78 (d, *J* = 4.0 Hz, 1H), 7.58–7.41 (m, 3H), 6.90 (s, 1H), 4.48–4.42 (m, 1H), 3.99–3.85 (m, 1H), 2.68 (s, 3H), 2.41–1.48 (m, 8H). LCMS (method LCMS8, ESI): *t*_R = 2.52 min, *m/z* = 411.1 [M + H]⁺.

(1*R*,3*R*)-3-(2-Methylimidazo[4,5-*d*]pyrrolo[2,3-*b*]pyridin-1(6*H*)-yl)cyclohexanol (20). An aqueous 1 M solution of sodium hydroxide (168 mL, 168 mmol) was added to a slurry of 20d (24.0 g, 58.5 mmol) in EtOH (240 mL) at room temperature. The reaction mixture was stirred at 50 °C for 18 h, then cooled to room temperature. The majority of the EtOH was removed under vacuum. Then the residual mixture was extracted with methyl ethyl ketone (2 × 250 mL). The combined organic layers were washed with brine (1 × 100 mL), then dried over magnesium sulfate and filtered. The filtrate was concentrated to dryness and then *i*-PrOH (50 mL) was added to the residue. After the resulting slurry was stirred at room temperature

for 24 h, the solid was isolated by filtration and dried under vacuum for 18 h to afford the title compound as a white solid (14.7 g, 93%). ¹H NMR (400 MHz, DMSO-*d*₆) δ: 11.77 (s, 1H), 8.44 (s, 1H), 7.43 (s, 1H), 6.67 (s, 1H), 4.79 (overlapping s and br s, 2H), 4.21 (s, 1H), 2.61 (s, 3H), 2.48–2.17 (m, 2H), 2.06–1.84 (m, 3H), 1.78 (d, *J* = 12.2 Hz, 1H), 1.74–1.58 (m, 2H). ¹³C NMR (125 MHz, DMSO-*d*₆) δ: 149.1, 144.2, 134.6, 131.9, 123.5, 104.0, 99.5, 64.6, 50.0, 36.9, 30.9, 29.8, 19.1, 14.4. LCMS (method LCMS4, ESI): *t*_R = 2.71 min, *m/z* = 271.1 [M + H]⁺. HRMS [M + H]⁺ expected, 271.1559; found, 271.1596.

cis-3-(2-Methylimidazo[4,5-*d*]pyrrolo[2,3-*b*]pyridin-1(6*H*)-yl)cyclohexanol (21). (±)-21 was synthesized by methods similar to those used for 20 and substituting (±)-*cis*-3-aminocyclohexanol (21a⁴⁸) for (1*R*,3*R*)-3-aminocyclohexanol (20a). 21 was separated from *ent*-21 by preparative chiral SFC (column, Phenomenex Lux Cellulose-2, 21.2 mm × 250 mm, 5 μm; detection, UV 220 nm; mobile phase A, CO₂; mobile phase B, EtOH containing 0.1% triethylamine; flow rate of 50 mL/min; gradient, isocratic, A/B = 70:30). Isolation and concentration of the appropriate fractions afforded two products with the following characteristics. For 21, white solid. Analytical chiral SFC (method SFC4): *t*_R = 0.85 min. ¹H NMR (400 MHz, DMSO-*d*₆) δ: 11.78 (s, 1H), 8.45 (s, 1H), 7.46 (t, *J* = 2.9 Hz, 1H), 6.69 (s, 1H), 4.87 (d, *J* = 4.9 Hz, 1H), 4.49 (br s, 1H), 3.74–3.63 (m, 1H), 2.61 (s, 3H), 2.28–2.02 (m, 3H), 1.97 (br d, *J* = 9.9 Hz, 1H), 1.89 (br d, *J* = 13.3 Hz, 1H), 1.83 (br d, *J* = 9.9 Hz, 1H), 1.59–1.27 (m, 2H). ¹³C NMR (125 MHz, DMSO-*d*₆) δ: 149.2, 144.2, 134.7, 134.2, 131.8, 123.5, 103.9, 99.7, 67.8, 52.9, 48.5, 34.2, 29.0, 21.7, 14.4. LCMS (method LCMS4, ESI) *t*_R = 2.63 min, *m/z* = 271.1 [M + H]⁺. HRMS [M + H]⁺ expected, 271.1559; found, 271.1571. For *ent*-21, white solid. Analytical chiral SFC (method SFC4): *t*_R = 0.71 min. ¹H NMR and LCMS data match those for 21.

trans-2-(2-Methylimidazo[4,5-*d*]pyrrolo[2,3-*b*]pyridin-1(6*H*)-yl)cyclohexanol (22). (±)-22 was synthesized by methods similar to those used for 20 and substituting (±)-*cis*-2-aminocyclohexanol (22a) for (1*R*,3*R*)-3-aminocyclohexanol (20a). 22 was separated from *ent*-22 by preparative chiral SFC (column, Chiralpak AD, 2.12 mm × 25 mm, 5 μm; detection, UV 220 nm; mobile phase A, CO₂; mobile phase B, MeOH; flow rate of 50 mL/min; gradient, isocratic, A/B = 60:40). Isolation and concentration of the appropriate fractions afforded two products with the following characteristics. For 22, white solid. Analytical chiral SFC (method SFC5): *t*_R = 0.74 min. ¹H NMR (400 MHz, DMSO-*d*₆) δ: 11.72 (s, 1H), 8.45 (s, 1H), 7.42 (s, 1H), 6.58 (s, 1H), 4.83 (d, *J* = 5.5 Hz, 1H), 4.28–4.16 (m, 1H), 4.14–4.06 (m, 1H), 2.58 (s, 3H), 2.41–2.30 (m, 1H), 2.10 (br d, *J* = 12.1 Hz, 1H), 1.95–1.73 (m, 3H), 1.65–1.38 (m, 3H). LCMS (method LCMS4, ESI) *t*_R = 2.87 min, *m/z* = 271.0 [M + H]⁺. For *ent*-22, white solid. Analytical chiral SFC (method SFC5): *t*_R = 0.52 min. ¹H NMR and LCMS data match those of 22.

trans-3-(2-Methylimidazo[4,5-*d*]pyrrolo[2,3-*b*]pyridin-1(6*H*)-yl)cyclopentanol (23). An amount of 1.6 g (3.1 mmol) of the *N*-*tert*-butyl carbamate protected precursor to (±)-*trans*-3-aminocyclopentanol (23a) was synthesized as previously described,⁴⁹ then treated with a 4 M solution of HCl in EtOAc (15 mL). The reaction mixture was stirred for 3 h at room temperature and then concentrated to dryness under vacuum. The crude residue was used immediately without further purification or characterization in the next step. (±)-23 was synthesized by methods similar to those used for 20 and substituting (±)-*trans*-3-aminocyclopentanol (23a) for (1*R*,3*R*)-3-aminocyclohexanol (20a). 23 was separated from *ent*-23 by preparative chiral SFC (column, Chiralpak AD, 30 mm × 250 mm, 5 μm; detection, UV 220 nm; mobile phase A, CO₂; mobile phase B, MeOH containing 0.2% DEA; flow rate of 50 mL/min; gradient, isocratic, A/B = 70:30). Isolation and concentration of the appropriate fractions afforded two products with the following characteristics. For 23, white solid. Analytical chiral SFC (method SFC6): *t*_R = 6.26 min. ¹H NMR (400 MHz, DMSO-*d*₆) δ: 11.81 (s, 1H), 8.46 (s, 1H), 7.43 (s, 1H), 6.43 (s, 1H), 5.28–5.21 (m, 1H), 4.92 (s, 1H), 4.51 (s, 1H), 2.61 (s, 3H), 2.49–2.32 (m, 2H), 2.28–2.12 (m, 2H), 2.05–1.97 (m, 1H), 1.81–1.71 (m, 1H). ¹³C NMR (125 MHz, DMSO-*d*₆) δ: 149.7, 144.1, 134.7, 134.1, 132.0, 123.7, 104.3, 97.9, 70.1, 54.8, 33.6, 27.8, 14.6. LCMS (method LCMS9, ESI) *t*_R = 0.77 min, *m/z* = 257.1 [M + H]⁺. HRMS

[M + H]⁺ expected, 257.1402; found, 257.1413. For *ent*-**23**, white solid. Analytical chiral SFC (method SFC6): *t*_R = 6.48 min. ¹H NMR and LCMS data match those of **23**.

cis-3-(2-Methylimidazo[4,5-d]pyrrolo[2,3-b]pyridin-1(6H)-yl)cyclopentanol (24). The *N*-*tert*-butyl carbamate protected precursor to (±)-*cis*-3-aminocyclopentanol (**24a**) was synthesized as previously described.⁴⁹ The *tert*-butyl carbamate protecting group was removed as described above for example **23**. (±)-**24** was synthesized by methods similar to those used for **20** and substituting (±)-*cis*-3-aminocyclopentanol (**24a**) for (1*R*,3*R*)-3-aminocyclohexanol (**20a**). **24** was separated from *ent*-**24** by preparative chiral SFC (column, Chiralpak AD, 30 mm × 250 mm, 20 μm; detection, UV 220 nm; mobile phase A, CO₂; mobile phase B, MeOH containing 0.2% DEA; flow rate of 50 mL/min; gradient, isocratic, A/B = 75:25). Isolation and concentration of the appropriate fractions afforded two products with the following characteristics. For **24**, white solid. Analytical chiral SFC (method SFC6): *t*_R = 6.65 min. ¹H NMR (400 MHz, DMSO-*d*₆) δ: 11.72 (s, 1H), 8.43 (s, 1H), 7.42–7.40 (m, 1H), 7.10–7.09 (m, 1H), 5.10 (d, *J* = 5.4 Hz, 1H), 4.89–4.85 (m, 1H), 4.38–4.35 (m, 1H), 2.60 (s, 3H), 2.49–2.41 (m, 2H), 2.22–2.14 (m, 1H), 1.98–1.91 (m, 2H), 1.88–1.83 (m, 1H). LCMS (method LCMS9, ESI) *t*_R = 0.86 min, *m/z* = 256.9 [M + H]⁺. For *ent*-**24**: white solid. Analytical chiral SFC (method SFC6): *t*_R = 6.80 min. ¹H NMR and LCMS data match those for **24**.

■ ASSOCIATED CONTENT

● Supporting Information

Details of analytical LCMS and SFC methods; experimental log *D* measurement procedures; thermodynamic solubility measurement procedures; in vitro and in vivo ADME experimental procedures; experimental details for IL6-induced pSTAT3 PK/PD study of compound **20** in the mouse; protein expression/purification and crystallographic methods and procedures for **3** (in complex with JAK2), **4** (in complex with JAK1 and JAK2), **20** (in complex with JAK1); details of JAK biochemical and cell-based assays; details of in vitro hERG assay; details of QM calculations and methods; biochemical inhibition of JAK3 and TYK2 by compounds **3–24**. This material is available free of charge via the Internet at <http://pubs.acs.org>.

Accession Codes

PDB codes are as follows: 4F08 for **3** complexed with JAK2; 4EHZ for **4** complexed with JAK1; 4F09 for **4** complexed with JAK2; 4E14 for **20** complexed with JAK1.

■ AUTHOR INFORMATION

Corresponding Author

*Phone: 650-467-4533. E-mail: mzak@gene.com.

Notes

The authors declare no competing financial interest.

■ ACKNOWLEDGMENTS

We thank Michael Hayes, Mengling Wong, Baiwei Lin, Deven Wang, Yutao Jiang, and Yanzhou Liu for purification and analytical support; Daniel Hascall, Grady Howes, Gigi Yuen, and Garima Porwal for compound management support; Hoa Le and Qin Yue for ADME support; Emile Plise and Jonathan Cheng for MDCK data; Erlie Delarosa for hepatocyte stability; Ning Liu for microsomal stability; Suzanne Tay for TDI studies; Jasleen Sodhi for reversible CYP inhibition measurement; Quynh Ho for plasma protein binding measurement; Paroma Chakravarty and Wei Jia for formulations support.

■ ABBREVIATIONS USED

ADME, absorption, distribution, metabolism, and excretion; aq, aqueous; ATP, adenosine triphosphate; AUC, area under the curve; b.i.d., twice daily; Bn, benzyl; Boc, *tert*-butyl carbamate; CL, clearance; *C*_{max}, maximum concentration; CYP, cytochrome P450; D, aspartic acid; DEA, diethylamine; DIPEA, *N,N*-diisopropylethylamine; E, glutamic acid; EC₅₀, half-maximal effective concentration; *ent*, enantiomer; EPO, erythropoietin; EtOAc, ethyl acetate; EtOH, ethanol; Ex, example; *F*, oral bioavailability; *F*_{max}, theoretical maximum achievable oral bioavailability; h, hour; HBD, hydrogen-bond donor; hERG, human ether-a-go-go-related gene; HPLC, high performance liquid chromatography; HRMS, high resolution mass spectrometry; IL-6, interleukin-6; *i*-PrOH, isopropyl alcohol; iv, intravenous; ip, intraperitoneal; JAK, Janus kinase; *K*_i(JAK2)/*K*_i(JAK1), JAK1 biochemical selectivity index; EC₅₀(EPO-pSTAT5)/EC₅₀(IL6-pSTAT3), JAK1 cellular selectivity index; *K*_i, inhibition constant; L, leucine; LCMS, liquid chromatography–mass spectrometry; log *D*_{7.2}, log of partition coefficient between octanol and pH 7.2 aqueous buffer; MCT, methylcellulose/Tween; MDCK, Madin–Darby canine kidney; MeOH, methanol; MF, myelofibrosis; min, minute; MsCl, methanesulfonyl chloride; N, asparagine; *P*_{app}, apparent permeability; PEG400, polyethylene glycol 400; PK, pharmacokinetics; PK/PD, pharmacokinetic/pharmacodynamic; po, by mouth; PPB, plasma protein binding; psi, pounds per square inch; *p*-TsOH, *p*-toluenesulfonic acid; R, arginine; RA, rheumatoid arthritis; S, serine; SFC, supercritical fluid chromatography; STAT, signal transducer and activator of transcription; QM, quantum mechanical; TFA, trifluoroacetic acid; THF, tetrahydrofuran; TPSA, topological polar surface area; UV, ultraviolet; Y, tyrosine

■ REFERENCES

- (1) Wilks, A. F.; Harpur, A. G.; Kurban, R. R.; Ralph, S. J.; Zurcher, G.; Ziemiecki, A. Two novel protein-tyrosine kinases, each with a second phosphotransferase-related catalytic domain, define a new class of protein kinase. *Mol. Cell. Biol.* **1991**, *11*, 2057–2065.
- (2) Harpur, A. G.; Andres, A. C.; Ziemiecki, A.; Aston, R. R.; Wilks, A. F. JAK2, a third member of the JAK family of protein tyrosine kinases. *Oncogene* **1992**, *7*, 1347–1353.
- (3) (a) Johnston, J. A.; Kawamura, M.; Kirken, R. A.; Chen, Y. Q.; Blake, T. B.; Shibuya, K.; Ortaldo, J. R.; McVicar, D. W.; O'Shea, J. J. Phosphorylation and activation of the Jak-3 Janus kinase in response to interleukin-2. *Nature* **1994**, *370*, 151–153. (b) Witthuhn, B. A.; Silvennoinen, O.; Miura, O.; Lai, K. S.; Cwik, C.; Liu, E. T.; Ihle, J. N. Involvement of the Jak-3 Janus kinase in signalling by interleukins 2 and 4 in lymphoid and myeloid cells. *Nature* **1994**, *370*, 153–157.
- (4) Firmbach-Kraft, I.; Byers, M.; Shows, T.; Dalla-Favera, R.; Krolewski, J. J. tyk2, prototype of a novel class of non-receptor tyrosine kinase genes. *Oncogene* **1990**, *5*, 1329–1336.
- (5) Huisling, M. O.; Kruiswijk, C. P.; Flik, G. Phylogeny and evolution of class-I helical cytokines. *J. Endocrinol.* **2006**, *189*, 1–25.
- (6) Bazan, J. F. Structural design and molecular evolution of a cytokine receptor superfamily. *Proc. Natl. Acad. Sci. U.S.A.* **1990**, *87*, 6934–6938.
- (7) (a) Darnell, J. E., Jr. STATs and gene regulation. *Science* **1997**, *277*, 1630–1635. (b) Darnell, J. E., Jr.; Kerr, I. M.; Stark, G. R. Jak-STAT pathways and transcriptional activation in response to IFNs and other extracellular signaling proteins. *Science* **1994**, *264*, 1415–1421. (c) O'shea, J. J.; Gadina, M.; Schreiber, R. D. Cytokine signaling in 2002: new surprises in the Jak/Stat pathway. *Cell* **2002**, *109* (Suppl.), S121–S131. (d) Schindler, C.; Levy, D. E.; Decker, T. JAK-STAT signaling: from interferons to cytokines. *J. Biol. Chem.* **2007**, *282*, 20059–20063.

- (8) (a) Ihle, J. N. STATs: signal transducers and activators of transcription. *Cell* **1996**, *84*, 331–334. (b) Baker, S. J.; Rane, S. G.; Reddy, E. P. Hematopoietic cytokine receptor signaling. *Oncogene* **2007**, *26*, 6724–6737.
- (9) (a) O’Shea, J. J. Jaks, STATs, cytokine signal transduction, and immunoregulation: Are we there yet? *Immunity* **1997**, *7*, 1–11. (b) Pesu, M.; Laurence, A.; Kishore, N.; Zwillich, S. H.; Chan, G.; O’Shea, J. J. Therapeutic targeting of Janus kinases. *Immunol. Rev.* **2008**, *223*, 132–142.
- (10) O’Shea, J. J.; Pesu, M.; Borie, D. C.; Changelian, P. S. A new modality for immunosuppression: targeting the JAK/STAT pathway. *Nat. Rev. Drug Discovery* **2004**, *3*, 555–564.
- (11) (a) Clark, S. C.; Kamen, R. The human hematopoietic colony-stimulating factors. *Science* **1987**, *236*, 1229–1237. (b) Metcalf, D. The molecular control of cell division, differentiation commitment and maturation in haemopoietic cells. *Nature* **1989**, *339*, 27–30. (c) Witthuhn, B. A.; Quelle, F. W.; Silvennoinen, O.; Yi, T.; Tang, B.; Miura, O.; Ihle, J. N. JAK2 associates with the erythropoietin receptor and is tyrosine phosphorylated and activated following stimulation with erythropoietin. *Cell* **1993**, *74*, 227–236.
- (12) Rochman, Y.; Spolski, R.; Leonard, W. J. New insights into the regulation of T cells by gamma(c) family cytokines. *Nat. Rev. Immunol.* **2009**, *9*, 480–490.
- (13) Noguchi, M.; Yi, H.; Rosenblatt, H. M.; Filipovich, A. H.; Adelstein, S.; Modi, W. S.; McBride, O. W.; Leonard, W. J. Interleukin-2 receptor gamma chain mutation results in X-linked severe combined immunodeficiency in humans. *Cell* **1993**, *73*, 147–157.
- (14) Stahl, N.; Boulton, T. G.; Farruggella, T.; Ip, N. Y.; Davis, S.; Witthuhn, B. A.; Quelle, F. W.; Silvennoinen, O.; Barbieri, G.; Pellegrini, S.; Ihle, J. N.; Yancopoulos, G. D. Association and activation of Jak-Tyk kinases by CNTF-LIF-OSM-IL-6 β receptor components. *Science* **1994**, *263*, 92–95.
- (15) Tanaka, T.; Kishimoto, T. Immunotherapeutic implication of IL-6 blockade. *Immunotherapy* **2012**, *4*, 87–105.
- (16) (a) Gouilleux, F.; Pallard, C.; Dusanter-Fourt, I.; Wakao, H.; Haldosen, L. A.; Norstedt, G.; Levy, D.; Groner, B. Prolactin, growth hormone, erythropoietin and granulocyte-macrophage colony stimulating factor induce MGF-Stat5 DNA binding activity. *EMBO J.* **1995**, *14*, 2005–2013. (b) Pallard, C.; Gouilleux, F.; Charon, M.; Groner, B.; Gisselbrecht, S.; Dusanter-Fourt, I. Interleukin-3, erythropoietin, and prolactin activate a STAT5-like factor in lymphoid cells. *J. Biol. Chem.* **1995**, *270*, 15942–15945. (c) Skoda, R. C. Specificity of signaling by hematopoietic cytokine receptors: instructive versus permissive effects. *J. Recept. Signal. Transduction Res.* **1999**, *19*, 741–772.
- (17) Wu, H.; Liu, X.; Jaenisch, R.; Lodish, H. F. Generation of committed erythroid BFU-E and CFU-E progenitors does not require erythropoietin or the erythropoietin receptor. *Cell* **1995**, *83*, 59–67.
- (18) Changelian, P. S.; Flanagan, M. E.; Ball, D. J.; Kent, C. R.; Magnuson, K. S.; Martin, W. H.; Rizzuti, B. J.; Sawyer, P. S.; Perry, B. D.; Brissette, W. H.; McCurdy, S. P.; Kudlacz, E. M.; Conklyn, M. J.; Elliott, E. A.; Koslov, E. R.; Fisher, M. B.; Strelevitz, T. J.; Yoon, K.; Whipple, D. A.; Sun, J.; Munchhof, M. J.; Doty, J. L.; Casavant, J. M.; Blumenkopf, T. A.; Hines, M.; Brown, M. F.; Lillie, B. M.; Subramanyam, C.; Shang-Poa, C.; Milici, A. J.; Beckius, G. E.; Moyer, J. D.; Su, C.; Woodworth, T. G.; Gaweco, A. S.; Beals, C. R.; Littman, B. H.; Fisher, D. A.; Smith, J. F.; Zagouras, P.; Magna, H. A.; Saltarelli, M. J.; Johnson, K. S.; Nelms, L. F.; Des Etages, S. G.; Hayes, L. S.; Kawabata, T. T.; Finco-Kent, D.; Baker, D. L.; Larson, M.; Si, M. S.; Paniagua, R.; Higgins, J.; Holm, B.; Reitz, B.; Zhou, Y. J.; Morris, R. E.; O’Shea, J. J.; Borie, D. C. Prevention of organ allograft rejection by a specific Janus kinase 3 inhibitor. *Science* **2003**, *302*, 875–878.
- (19) Flanagan, M. E.; Blumenkopf, T. A.; Brissette, W. H.; Brown, M. F.; Casavant, J. M.; Shang-Poa, C.; Doty, J. L.; Elliott, E. A.; Fisher, M. B.; Hines, M.; Kent, C.; Kudlacz, E. M.; Lillie, B. M.; Magnuson, K. S.; McCurdy, S. P.; Munchhof, M. J.; Perry, B. D.; Sawyer, P. S.; Strelevitz, T. J.; Subramanyam, C.; Sun, J.; Whipple, D. A.; Changelian, P. S. Discovery of CP-690,550: a potent and selective Janus kinase (JAK) inhibitor for the treatment of autoimmune diseases and organ transplant rejection. *J. Med. Chem.* **2010**, *53*, 8468–8484.
- (20) (a) Fleischmann, R.; Cutolo, M.; Genovese, M. C.; Lee, E. B.; Kanik, K. S.; Sadis, S.; Connell, C. A.; Gruben, D.; Krishnaswami, S.; Wallenstein, G.; Wilkinson, B. E.; Zwillich, S. H. Phase 2B dose-ranging study of the oral JAK inhibitor tofacitinib (CP-690,550) or adalimumab monotherapy versus placebo in patients with active rheumatoid arthritis with an inadequate response to DMARDs. *Arthritis Rheum.* **2012**, *64*, 617–629. (b) Kremer, J. M.; Cohen, S.; Wilkinson, B. E.; Connell, C. A.; French, J. L.; Gomez-Reino, J.; Gruben, D.; Kanik, K. S.; Krishnaswami, S.; Pascual-Ramos, V.; Wallenstein, G.; Zwillich, S. H. A phase 2B dose-ranging study of the oral JAK inhibitor tofacitinib (CP-690,550) versus placebo in combination with background methotrexate in patients with active rheumatoid arthritis and inadequate response to methotrexate alone. *Arthritis Rheum.* **2011**, *64*, 970–981.
- (21) Tofacitinib has completed several late stage clinical trials and recently received a recommendation for approval in RA from the FDA Advisory Committee.
- (22) Lin, Q.; Meloni, D.; Pan, Y.; Xia, M.; Rodgers, J.; Shepard, S.; Li, M.; Galya, L.; Metcalf, B.; Yue, T. Y.; Liu, P.; Zhou, J. Enantioselective synthesis of Janus kinase inhibitor INCB018424 via an organocatalytic aza-Michael reaction. *Org. Lett.* **2009**, *11*, 1999–2002.
- (23) (a) Williams, W. V.; Scherle, P.; Shi, J.; Newton, R.; McKeever, E.; Fridman, J.; Vaddi, K.; Levy, R.; Moreland, L. Initial efficacy of INCB018424, a selective janus kinase 1 & 2 (JAK1&2) inhibitor in rheumatoid arthritis (RA). *Ann. Rheum. Dis.* **2008**, *67* (Suppl. 2), 62. The abstract is online at http://www.abstracts2view.com/eular/view.php?nu=EULAR08L_OP-0044 (accessed May 30, 2012). (b) A Study Exploring the Safety, Tolerability and Efficacy of a 4 Week Course of INCB018424 in Subjects with Active Rheumatoid Arthritis. <http://www.clinicaltrials.gov/ct2/show/NCT00550043?term=incb018424&rank=19> (accessed June 5, 2012).
- (24) (a) In addition to being studied in early stage trials for RA, ruxolitinib has also been extensively evaluated as a treatment for myelofibrosis (MF). Recently, the Food and Drug Administration (FDA) granted marketing approval to ruxolitinib as a treatment for patients with MF. Incyte Press Release. <http://investor.incyte.com/phoenix.zhtml?c=69764&p=irol-newsArticle&ID=1631201&highlight> (accessed May 30, 2012). (b) Incyte and Eli Lilly have progressed another small molecule JAK1/2 inhibitor (INCB028050/LY3009104) into clinical trials for rheumatoid arthritis. Greenwald, M. W.; Fidelus-Gort, R.; Levy, R.; Liang, J.; Vaddi, K.; Williams, W. V.; Newton, R. A randomized dose-ranging, placebo-controlled study of INCB028050, a selective JAK1 and JAK2 inhibitor in subjects with active rheumatoid arthritis. *Arthritis Rheum.* **2010**, *62* (Suppl. 10), 2172. (c) Further information on a phase 2a clinical trial of INCB028050/LY3009104 may be found in an Incyte press release: <http://investor.incyte.com/phoenix.zhtml?c=69764&p=irol-newsArticle&ID=1494997&highlight=> (accessed June 6, 2012).
- (25) (a) Meyer, D. M.; Jesson, M. I.; Li, X.; Elrick, M. M.; Funches-Shippy, C. L.; Warner, J. D.; Gross, C. J.; Dowty, M. E.; Ramaiah, S. K.; Hirsch, J. L.; Saabye, M. J.; Barks, J. L.; Kishore, N.; Morris, D. L. Anti-inflammatory activity and neutrophil reductions mediated by the JAK1/JAK3 inhibitor, CP-690,550, in rat adjuvant-induced arthritis. *J. Inflammation (London, U. K.)* **2010**, *7*, 41. (b) Thoma, G.; Nuninger, F.; Falchetto, R.; Hermes, E.; Tavares, G. A.; Vangrevelinghe, E.; Zerwes, H. G. Identification of a potent Janus kinase 3 inhibitor with high selectivity within the Janus kinase family. *J. Med. Chem.* **2011**, *54*, 284–288.
- (26) Quintas-Cardama, A.; Vaddi, K.; Liu, P.; Manshour, T.; Li, J.; Scherle, P. A.; Caulder, E.; Wen, X.; Li, Y.; Waeltz, P.; Rupar, M.; Burn, T.; Lo, Y.; Kelley, J.; Covington, M.; Shepard, S.; Rodgers, J. D.; Haley, P.; Kantarjian, H.; Fridman, J. S.; Verstovsek, S. Preclinical characterization of the selective JAK1/2 inhibitor INCB018424: therapeutic implications for the treatment of myeloproliferative neoplasms. *Blood* **2010**, *115*, 3109–3117.
- (27) Van Abbema, A.; Kanada, H.; Chang, C.; Bir Kohli, P.; Smith, J.; Barrett, K.; Lewin-Koh, N.; Johnson, A. R.; Ghilardi, N.; Blair, W. Determination of the JAK-dependence of cytokine pathways using small molecule inhibitors. Unpublished results. Experimental details of

the biochemical and cell-based assays reported herein may be found in the Supporting Information.

(28) Rodig, S. J.; Meraz, M. A.; White, J. M.; Lampe, P. A.; Riley, J. K.; Arthur, C. D.; King, K. L.; Sheehan, K. C.; Yin, L.; Pennica, D.; Johnson, E. M., Jr.; Schreiber, R. D. Disruption of the Jak1 gene demonstrates obligatory and nonredundant roles of the Jaks in cytokine-induced biologic responses. *Cell* **1998**, *93*, 373–383.

(29) Shimoda, K.; Kouji, K.; Aoki, K.; Matsuda, T.; Miyamoto, A.; Shibamori, M.; Yamashita, M.; Numata, A.; Takase, K.; Kobayashi, S.; Shibata, S.; Asano, Y.; Gondo, H.; Sekiguchi, K.; Nakayama, K.; Nakayama, T.; Okamura, T.; Okamura, S.; Niho, Y.; Nakayama, K. Tyk2 plays a restricted role in IFN α signaling, although it is required for IL-12-mediated T cell function. *Immunity* **2000**, *13*, 561–571.

(30) Parganas, E.; Wang, D.; Stravopodis, D.; Topham, D. J.; Marine, J. C.; Teglund, S.; Vanin, E. F.; Bodner, S.; Colamonici, O. R.; van Deursen, J. M.; Grosveld, G.; Ihle, J. N. Jak2 is essential for signaling through a variety of cytokine receptors. *Cell* **1998**, *93*, 385–395.

(31) Smolen, J. S.; Beaulieu, A.; Rubbert-Roth, A.; Ramos-Remus, C.; Rovinsky, J.; Alecock, E.; Woodworth, T.; Alten, R. Effect of interleukin-6 receptor inhibition with tocilizumab in patients with rheumatoid arthritis (OPTION study): a double-blind, placebo-controlled, randomised trial. *Lancet* **2008**, *371*, 987–997.

(32) Haan, C.; Rolving, C.; Raulf, F.; Kapp, M.; Druckes, P.; Thoma, G.; Behrmann, I.; Zerwes, H. G. Jak1 has a dominant role over Jak3 in signal transduction through γ c-containing cytokine receptors. *Chem. Biol.* **2011**, *18*, 314–323.

(33) (a) Frenzel, K.; Wallace, T. A.; McDoom, I.; Xiao, H. D.; Capocchi, M. R.; Bernstein, K. E.; Sayeski, P. P. A functional Jak2 tyrosine kinase domain is essential for mouse development. *Exp. Cell Res.* **2006**, *312*, 2735–2744. (b) Neubauer, H.; Cumano, A.; Muller, M.; Wu, H.; Huffstadt, U.; Pfeffer, K. Jak2 deficiency defines an essential developmental checkpoint in definitive hematopoiesis. *Cell* **1998**, *93*, 397–409.

(34) Verstovsek, S.; Kantarjian, H.; Mesa, R. A.; Pardanani, A. D.; Cortes-Franco, J.; Thomas, D. A.; Estrov, Z.; Fridman, J. S.; Bradley, E. C.; Erickson-Viitanen, S.; Vaddi, K.; Levy, R.; Tefferi, A. Safety and efficacy of INCB018424, a JAK1 and JAK2 inhibitor, in myelofibrosis. *N. Engl. J. Med.* **2010**, *363*, 1117–1127.

(35) A summary of previous disclosures of compounds exhibiting JAK1 vs JAK2 selectivity is presented in ref 36. Additionally, a number of publications describing JAK2 inhibitors with varying JAK family and other kinase selectivity profiles have appeared recently. These include the following: (a) Schenkel, L. B.; Huang, X.; Cheng, A.; Deak, H. L.; Doherty, E.; Emkey, R.; Gu, Y.; Gunaydin, H.; Kim, J. L.; Lee, J.; Loberg, R.; Olivieri, P.; Pistillo, J.; Tang, J.; Wan, Q.; Wang, H. L.; Wang, S. W.; Wells, M. C.; Wu, B.; Yu, V.; Liu, L.; Geuns-Meyer, S. Discovery of potent and highly selective thienopyridine Janus kinase 2 inhibitors. *J. Med. Chem.* **2011**, *54*, 8440–8450. (b) Lim, J.; Taoka, B.; Otte, R. D.; Spencer, K.; Dinsmore, C. J.; Altman, M. D.; Chan, G.; Rosenstein, C.; Sharma, S.; Su, H. P.; Szwczak, A. A.; Xu, L.; Yin, H.; Zuyag-Murphy, J.; Marshall, C. G.; Young, J. R. Discovery of 1-amino-5H-pyrido[4,3-b]indol-4-carboxamide inhibitors of Janus kinase 2 (JAK2) for the treatment of myeloproliferative disorders. *J. Med. Chem.* **2011**, *54*, 7334–7349. (c) Siu, T.; Kozina, E. S.; Jung, J.; Rosenstein, C.; Mathur, A.; Altman, M. D.; Chan, G.; Xu, L.; Bachman, E.; Mo, J. R.; Bouthilllette, M.; Rush, T.; Dinsmore, C. J.; Marshall, C. G.; Young, J. R. The discovery of tricyclic pyridone JAK2 inhibitors. Part 1: Hit to lead. *Bioorg. Med. Chem. Lett.* **2010**, *20*, 7421–7425. (d) William, A. D.; Lee, A. C.; Blanchard, S.; Poulsen, A.; Teo, E. L.; Nagaraj, H.; Tan, E.; Chen, D.; Williams, M.; Sun, E. T.; Goh, K. C.; Ong, W. C.; Goh, S. K.; Hart, S.; Jayaraman, R.; Pasha, M. K.; Ethirajulu, K.; Wood, J. M.; Dymock, B. W. Discovery of the macrocycle 11-(2-pyrrolidin-1-yl-ethoxy)-14,19-dioxo-5,7,26-triazao-tetracyclo[19.3.1.1(2,6).1(8,12)]-heptacos-1(25),2(26),3,5,8,10,12(27),16,21,23-decaene (SB1518), a potent Janus kinase 2/Fms-like tyrosine kinase-3 (JAK2/FLT3) inhibitor for the treatment of myelofibrosis and lymphoma. *J. Med. Chem.* **2011**, *54*, 4638–4658. (e) Ioannidis, S.; Lamb, M. L.; Wang, T.; Almeida, L.; Block, M. H.; Davies, A. M.; Peng, B.; Su, M.; Zhang, H. J.; Hoffmann, E.; Rivard, C.; Green, L.; Howard, T.; Pollard, H.; Read,

J.; Alimzhanov, M.; Bebernitz, G.; Bell, K.; Ye, M.; Huszar, D.; Zinda, M. Discovery of 5-chloro-N2-[(1S)-1-(5-fluoropyrimidin-2-yl)ethyl]-N4-(5-methyl-1H-pyrazol-3-yl)pyrimidine-2,4-diamine (AZD1480) as a novel inhibitor of the Jak/Stat pathway. *J. Med. Chem.* **2011**, *54*, 262–276. (f) Wernig, G.; Kharas, M. G.; Okabe, R.; Moore, S. A.; Leeman, D. S.; Cullen, D. E.; Gozo, M.; McDowell, E. P.; Levine, R. L.; Doukas, J.; Mak, C. C.; Noronha, G.; Martin, M.; Ko, Y. D.; Lee, B. H.; Soll, R. M.; Tefferi, A.; Hood, J. D.; Gilliland, D. G. Efficacy of TG101348, a selective JAK2 inhibitor, in treatment of a murine model of JAK2V617F-induced polycythemia vera. *Cancer Cell* **2008**, *13*, 311–320. (g) Burns, C. J.; Bourke, D. G.; Andrau, L.; Bu, X.; Charman, S. A.; Donohue, A. C.; Fantino, E.; Farrugia, M.; Feutrell, J. T.; Joffe, M.; Kling, M. R.; Kurek, M.; Nero, T. L.; Nguyen, T.; Palmer, J. T.; Phillips, I.; Shackelford, D. M.; Sikanyika, H.; Styles, M.; Su, S.; Treutlein, H.; Zeng, J.; Wilks, A. F. Phenylaminopyrimidines as inhibitors of Janus kinases (JAKs). *Bioorg. Med. Chem. Lett.* **2009**, *19*, 5887–5892. (h) Hexner, E. O.; Serdikoff, C.; Jan, M.; Swider, C. R.; Robinson, C.; Yang, S.; Angeles, T.; Emerson, S. G.; Carroll, M.; Ruggeri, B.; Dobrzanski, P. Lestaurtinib (CEP701) is a JAK2 inhibitor that suppresses JAK2/STAT5 signaling and the proliferation of primary erythroid cells from patients with myeloproliferative disorders. *Blood* **2008**, *111*, 5663–5671.

(36) Kulagowski, J. J.; Blair, W.; Bull, R. J.; Chang, C.; Deshmukh, G.; Dyke, H. J.; Eigenbrot, C.; Ghilardi, N.; Gibbons, P.; Harrison, T. K.; Hewitt, P. R.; Liimatta, M.; Hurley, C. A.; Johnson, A.; Johnson, T.; Kenny, J. R.; Bir Kohli, P.; Maxey, R. J.; Mendonca, R.; Mortara, K.; Murray, J.; Narukulla, R.; Shia, S.; Steffek, M.; Ubhayakar, S.; Ultsch, M.; van Abbema, A.; Ward, S. I.; Waszkowycz, B.; Zak, M. Identification of imidazo-pyrrolopyridines as novel and potent JAK1 Inhibitors. *J. Med. Chem.* [Online early access]. DOI: 10.1021/jm300438j. Published online: May 16, 2012.

(37) Prior to commencement of our work, a series of related, imidazolone-containing compounds had been described as JAK3 inhibitors: (a) Inoue, T.; Tanaka, A.; Nakai, K.; Sasaki, H.; Takahashi, F.; Shirakami, S.; Hatanaka, K.; Nakajima, Y.; Mukoyoshi, K.; Hamaguchi, H.; Kunikawa, S.; Higashi, Y. Heterocyclic Janus Kinase 3 Inhibitors. WO2007077949, 2007. More recently, during the course of or after completion of our work, patent applications have appeared describing other tricyclic azaindole-containing scaffolds as JAK inhibitors. These include azaindole annelated by pyrrole: (b) Shirakami, S.; Nakajima, Y.; Maeda, J.; Tominaga, H.; Yamagishi, H.; Hondo, T.; Inami, M.; Morio, H.; Inoue, T.; Mizutani, T.; Ishioka, H. Fused Pyrrolopyridine Derivative. WO2010119875, 2010. Azaindole annelated by pyrrole, pyrazole, and isoxazole: (c) Wishart, N.; Argiriadi, M.; Calderwood, D. J.; Ericsson, A. M.; Fiamengo, B. A.; Frank, K. E.; Friedman, M.; George, D. M.; Goedken, E. R.; Josephsohn, N. S.; Li, B. C.; Morytko, M. J.; Stewart, K. D.; Voss, J. W.; Wallace, G. A.; Wang, L.; Woller, K. R. Novel Tricyclic Compounds. WO2009152133, 2009. Azaindole annelated by isothiazole, triazole, and imidazole: (d) Wishart, N.; Argiriadi, M.; Breinlinger, E. C.; Calderwood, D. J.; Ericsson, A. M.; Fiamengo, B. A.; Frank, K. E.; Friedman, M.; George, D. M.; Goedken, E. R.; Josephsohn, N. S.; Li, B. C.; Morytko, M. J.; Mullen, K. D.; Somal, G.; Stewart, K. D.; Voss, J. W.; Wallace, G. A.; Wang, L.; Woller, K. R. Novel Tricyclic Compounds. WO2011068899, 2011. Tricyclic systems related to 3 but having distinct substitution on the core and probably employing an alternative hinge-binding mode have recently appeared as JAK2 inhibitors: (e) Purandare, A. V.; Grebinski, J. W.; Hart, A.; Inghrim, J.; Schroeder, G.; Wan, H. JAK2 Inhibitors and Their Use for the Treatment of Myeloproliferative Diseases and Cancer. WO2011028864, 2011.

(38) EC₅₀ values for compounds that do not achieve at least 50% inhibition at the highest concentration tested (10000 nM) in the cell based assays are considered to be noncalculable and are reported as >10000 nM. Because of normal run-to-run variability, some weakly potent compounds achieve >50% inhibition in some, but not all, of the replicate runs. In these cases, we report EC₅₀ > X, where X is the arithmetic mean of all the individual EC₅₀ values, both calculable and noncalculable. For example, compound 3 displayed replicate EC₅₀

values of 6300, >10000, and >10000 nM in the EPO-pSTAT5 assay; thus, the average EC_{50} is reported as >8800 nM.

(39) Ertl, P.; Rohde, B.; Selzer, P. Fast calculation of molecular polar surface area as a sum of fragment-based contributions and its application to the prediction of drug transport properties. *J. Med. Chem.* **2000**, *43*, 3714–3717.

(40) Prior to synthesis, predicted log D values were calculated using the MoKa software (www.moldiscovery.com (ref 40a) and a custom pK_a model (ref 40b). (a) Milletti, F.; Storchi, L.; Sforza, G.; Cruciani, G. New and original pK_a prediction method using grid molecular interaction fields. *J. Chem. Inf. Model.* **2007**, *47*, 2172–2181. (b) Milletti, F.; Storchi, L.; Goracci, L.; Bendels, S.; Wagner, B.; Kansy, M.; Cruciani, G. Extending pK_a prediction accuracy: high-throughput pK_a measurements to understand pK_a modulation of new chemical series. *Eur. J. Med. Chem.* **2010**, *45*, 4270–4279.

(41) The t tests were conducted on the JAK1 and JAK2 K_i values for **4**, **11**, **14**, and **20**. In each case, JAK1 biochemical activity was found to be inhibited to a greater extent than the corresponding JAK2 biochemical activity by a statistically significant margin ($p < 0.02$ for **14**, $p < 0.001$ for **4**, **11**, and **20**).

(42) Balague, C.; Pont, M.; Prats, N.; Godessart, N. Profiling of dihydroorotate dehydrogenase, p38 and JAK inhibitors in the rat adjuvant-induced arthritis model: a translational study. *Br. J. Pharmacol.* **2012**, *166*, 1320–1332.

(43) The maximum achievable oral bioavailability (F_{max}) is the product of the fraction absorbed (F_a), the fraction escaping intestinal metabolism (F_g), and the fraction escaping hepatic metabolism (F_h), as expressed by the equation $F_{max} = F_a F_g F_h$. Assuming a best case scenario of no intestinal wall metabolism and complete absorption of the oral dose (F_g and F_a are 1), the equation is simplified to $F_{max} = F_h$. Since $F_h = 1 - CL/Q_h$, where CL is clearance and Q_h is hepatic blood flow, it is apparent that the maximum achievable bioavailability should be controlled by clearance according to the equation $F_{max} = 1 - CL/Q_h$. Assuming a hepatic blood flow in the rat of $70 \text{ mL min}^{-1} \text{ kg}^{-1}$, a compound with an iv clearance of $43 \text{ mL min}^{-1} \text{ kg}^{-1}$ should have an F_{max} of 39%. See the following: Rautio, J.; Kumpulainen, H.; Heimbach, T.; Oliyai, R.; Oh, D.; Järvinen, T.; Savolainen, J. Prodrugs: design and clinical applications. *Nat. Rev. Drug Discovery* **2008**, *7*, 255–270.

(44) (a) Bondi, D. van der Waals volumes and radii. *J. Phys. Chem.* **1964**, *68*, 441–451. (b) Li, A.; Nussinov, R. A set of van der Waals and coulombic radii of protein atoms for molecular and solvent-accessible surface calculation, packing evaluation and docking. *Proteins: Struct., Funct., Genet.* **1998**, *32*, 111–127.

(45) Further details on the quantum mechanical calculations may be found in the Supporting Information.

(46) (a) van Niel, M. B.; Collins, I.; Beer, M. S.; Broughton, H. B.; Cheng, S. K.; Goodacre, S. C.; Heald, A.; Locker, K. L.; MacLeod, A. M.; Morrison, D.; Moyes, C. R.; O'Connor, D.; Pike, A.; Rowley, M.; Russell, M. G.; Sohal, B.; Stanton, J. A.; Thomas, S.; Verrier, H.; Watt, A. P.; Castro, J. L. Fluorination of 3-(3-(piperidin-1-yl)propyl)indoles and 3-(3-(piperazin-1-yl)propyl)indoles gives selective human 5-HT1D receptor ligands with improved pharmacokinetic profiles. *J. Med. Chem.* **1999**, *42*, 2087–2104. (b) Basarab, G.; Ni, H.; Sherer, B.; Zhou, F. Chemical Compounds. WO2007071965, 2007.

(47) (a) Shirakami, S.; Takayuki, I.; Mukoyoshi, K.; Nakajima, Y.; Usuda, H.; Hamaguchi, H.; Higashi, Y.; Hatanaka, K. Condensed Pyridine Compounds. EP2123651, 2009. (b) Remen, L.; Bezencon, O.; Richard-Bildstein, S.; Bur, D.; Prade, L.; Corminboeuf, O.; Boss, C.; Grisostomi, C.; Sifferlen, T.; Strickner, P.; Hess, P.; Delahaye, S.; Treiber, A.; Weller, T.; Binkert, C.; Steiner, B.; Fischli, W. New classes of potent and bioavailable human renin inhibitors. *Bioorg. Med. Chem. Lett.* **2009**, *19*, 6762–6765.

(48) Brocklehurst, C. E.; Laumen, K.; La Vecchia, L.; Shaw, D.; Vögtle, M. Diastereoisomeric salt formation and enzyme-catalyzed kinetic resolution as complementary methods for the chiral separation of *cis*-/*trans*-enantiomers of 3-aminocyclohexanol. *Org. Process Res. Dev.* **2011**, *15*, 294–300.

(49) Erickson, S. D.; Qjan, Y.; Tilley, J. W. Diaminocyclohexane and Diaminocyclopentane Derivatives. WO2008065021, 2008.